Analysis of a drill core from the central uplift of Flynn Creek impact structure, Tennessee

by

David Rollin Adrian

A thesis submitted to the Graduate Faculty of
Auburn University
in partial fulfillment of the
requirements for the Degree of
Master of Science

Auburn, Alabama
May 7, 2017

Keywords: Flynn Creek, line-logging, central uplift,
impact crater, cryptocrystalline melt, resurge

Approved by

Dr. David T. King Jr, Chair, Professor of Geology
Dr. Willis E. Hames, Professor of Geology
Dr. Ashraf Uddin, Professor of Geology

Abstract

Flynn Creek impact structure is a small, asymmetric marine impact structure located in north-central Tennessee that formed when a hypervelocity impact occurred in an ancient shallow marine environment, with the target strata ranging from Lower to Upper Ordovician carbonates. Like other, similarly sized marine-target impact craters, Flynn Creek's structure-filling deposits consist of gravity-driven avalanche material, washed-back ejecta, and aqueous settling deposits. Sedimentological and petrographic analysis of drill core FC77-1, located on the western flank of the central uplift, led to the distinction of three sedimentological units, a generally fining-upward sequence from 109 to 32 m depth bounded by generally coarsening-upward sequences, within the upper 175-m interval of the core. Line-logging and thin-section analysis of selected drill core samples also show that the Flynn Creek impact breccia consists almost entirely of dolostone clasts (90%), with minor components of cryptocrystalline melt clasts, chert and shale fragments, and clastic grains. Cryptocrystalline melt clasts, the first melt clasts of any kind to be reported from Flynn Creek impact structure, appear isotropic in thin section, are in fact made of exceedingly fine quartz crystals.

Resurge gullies and an 'inverted sombrero,' an annular, sloping surface, are two geomorphic features sometimes referred to in studies of other marine-target impact structures, but have yet to be described at Flynn Creek. In this report, these features are related to marine crater formation and Flynn Creek is compared to similarly sized marine-target impact structures.

Acknowledgments

I would like to thank the National Aeronautics and Space Administration, Planetary Geology and Geophysics Program, for supporting the project proposal (NASA PGG NNH14AY73I) and the subcontract support from the USGS Astrogeology Science Center, Flagstaff. I would also like to thank the USGS Astrogeology Science Center, Flagstaff for the creation and organization of the Flynn Creek drill-core collection and providing data, documents, many forms of assistance in sampling, and hosting our visits to work on these materials. A big thank you goes out to Dr. David King Jr., Dr. Jens Ormö, Dr. Donn Rodekohr, Benjamin Swan, Steven Jaret, and Rebecca Koch, all of which helped with the collection, manipulation, and analysis of data, whether it was line-logging, core descriptions, photography, geophysical or statistical analysis. My advisor Dr. David King Jr. has been an integral part of my successes over the past few years and he continues to shape the way I approach science as a whole. Due to him initially giving me the opportunity to work within the realm of impact craters and teach Concepts of Science lab sections, I now feel I have found not one, but two strong interests. At home, my fiancée Rebecca and our corgis Colby and Daisy kept me grounded while I traversed the unpredictable and sometimes maddening world of graduate school. Growing up in Auburn, my parents were always a short distance away, or at least a phone call, no matter the hour and no matter the topic.

Table of Contents

List of Tables

List of Figures

Introduction

This thesis is part of a multi-year, collaborative project between teams at the USGS Astrogeology Science Center in Flagstaff, Arizona and Auburn University, led by Dr. Justin Hagerty and Dr. David King Jr, respectively, with the goal to reconstruct the origin and evolution of Flynn Creek impact structure by combining core description and in-depth petrographic analysis, microbeam imaging techniques, bulk rock and microbeam geochemical analysis, and numerical modeling.

Following a manuscript format, as outlined by the Department of Geosciences at Auburn University, this thesis comprises two papers written in the *Meteoritics and Planetary Science*'s format. The first paper, "Sedimentological and petrographic analysis of drill core FC77-1 from the flank of the central uplift, Flynn Creek impact structure, Tennessee," which has been accepted for publication in *Meteoritics and Planetary Science* and is currently going through revisions in typesetting, explores the sequence of events related to the formation of the Flynn Creek impact structure, specifically the central uplift, by using grain-size analysis and detailed petrographic descriptions. The second paper, "Resurge gullies and the 'inverted sombrero' rim at Flynn Creek impact structure, Tennessee," is to be submitted to *Meteoritics and Planetary Science*. This paper uses geographic information system (GIS) technology to assess two important geomorphic features, relate them to the marine environment present during the formation of this marine impact structure, and ultimately compare the Flynn Creek impact structure with other marine-target impact structures.

Additional data (an inventory of information about the thin sections made for this study and geochemical data from selected drill core samples), which were not included in either paper, has been added to the present report as an appendix and will also be archived at the Department of Geosciences at Auburn University.

CHAPTER 1

Sedimentological and petrographic analysis of drill core FC77-1 from the flank of the central uplift, Flynn Creek impact structure, Tennessee

David R. ADRIAN[1], David T. KING Jr.[1], Steven J. JARET[2], Jens ORMÖ[3], Lucille W. PETRUNY[1], Justin J. HAGERTY[4], and Tenielle A. GAITHER[4]

[1]Deptartment of Geosciences, Auburn University, Auburn, Alabama 36849

[2]Department of Geosciences, Stony Brook University, Stony Brook, New York 11794

[3]Centro de Astrobiología (INTA-CSIC), Madrid, Spain

[4]USGS, Astrogeology Science Center, Flagstaff, Arizona 86001

Abstract – Drill core FC77-1 on the flank of the central uplift, Flynn Creek impact structure, Tennessee, contains 175 m of impact breccia lying upon uplifted Lower Paleozoic carbonate target stratigraphy. Sedimentological analysis of this 175-m interval carbonate breccia shows that there are three distinct sedimentological units. In stratigraphic order, unit 1 (175 to 109 m) is an overall coarsening-upward section, whereas the overlying unit 2 (109 to 32 m) is overall fining-upward. Unit 3 (32 to 0 m) is a coarsening-upward sequence that is truncated at the top by erosion. Units 1 and 3 are interpreted as debris or rock avalanches into finer sedimentary deposits within intra-crater marine waters, thus producing progressively coarser, coarsening-upward sequences. Unit 2 is interpreted to have formed by debris or rock avalanches into standing marine waters, thus forming sequential fining-upward deposits. Line-logging of clasts ranging from 5 mm to 1.6 m, and thin-section analysis of selected drill core samples (including clasts < 5 mm), both show that the Flynn Creek impact breccia consists almost entirely of

dolostone clasts (90%), with minor components of cryptocrystalline melt clasts, chert and shale fragments, and clastic grains. Cryptocrystalline melt clasts, which appear isotropic in thin section, are in fact made of exceedingly fine quartz crystals that exhibit micro-Fourier Transform Infrared (FTIR) and micro-Raman spectra consistent with crystalline quartz. These cryptocrystalline melt clasts are the first melt clasts of any kind to be reported from Flynn Creek impact structure.

INTRODUCTION

The Flynn Creek impact structure, ~ 3.8 km in diameter and located in Jackson County, Tennessee (36° 17' N; 85° 40' W), is situated within the Eastern Highland Rim physiographic province of Tennessee (Conant and Swanson, 1961). This crater has an asymmetric outline and displays a central uplift, breccia moat, and terraced crater rim (Roddy, 1968; 1979; Schieber and Over, 2005; Evenick and Hatcher, 2007). Figure 1 shows the geologic setting of the Flynn Creek area and the impact structure's asymmetric outline, as inferred from the detailed reconnaissance of Roddy (1966; 1968).

The target stratigraphic section was essentially flat-lying, Ordovician carbonates ranging from Lower Ordovician Knox Group through Upper Ordovician Catheys-Leipers Formation (Roddy, 1968; 1979; Evenick and Hatcher, 2007; Gaither et al., 2015). Figure 2 shows the target stratigraphy and its age relationships, plus information on the thicknesses and general petrology of the units. The Knox Group is approximately 1 km thick in the target area (Roddy, 1968), which suggests that impact deformation does not extend below the Knox itself.

Almost all crater-rim exposures consist of Catheys-Leipers Formation of the target section, whereas the central uplift exposures consist primarily of target Knox and Stones River Groups (Roddy, 1968; 1979; Evenick and Hatcher, 2007; Gaither et al., 2015). In a subsequent,

post-impact phase, Upper Devonian Chattanooga Shale was deposited within the impact structure and across the area on what was then a shallow marine shelf (Roddy, 1968; 1979; Schieber and Over, 2005; Evenick and Hatcher, 2007; Gaither et al., 2015).

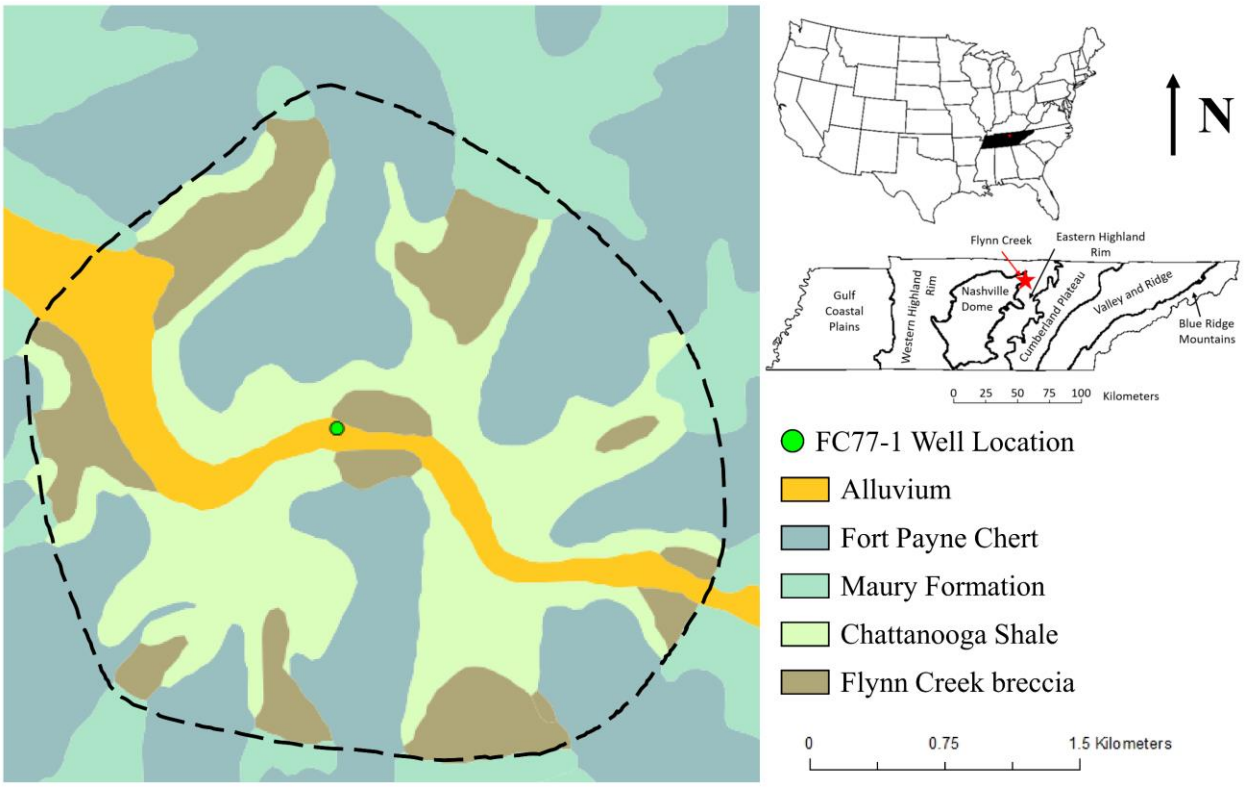

Figure 1. Geological map of Flynn Creek impact structure and vicinity. Inset maps show the location of the state of Tennessee in the contiguous United States and the location of the Flynn Creek impact structure on the margin of the Nashville Dome (Eastern Highland Rim area). Green dot show the location of core hole FC77-1 of this study. Colors show the main stratigraphic units, including alluvium and the Fort Payne Formation (post-impact chert), Maury Formation (post-impact shale), Chattanooga Shale (post-impact shale) and Flynn Creek breccia (crater-filling unit). The outcrops of the Catheys-Leipers Formation in the rim area and the Stones River and Knox Groups in the central uplift area are too small to show at this scale. The central uplift is indicated by the central outcrop of Flynn Creek impact breccia (brown), which caps the exposure of the central peak and its flanks. Dashed line shows the asymmetric limit of the impact structure's rim according to Roddy (1968), who conducted extensive field studies in the area. Modified from the Flynn Creek map on the U.S. Geological Survey Mineral Resources On-Line Spatial Database (U. S. Geological Survey, 2017).

PREVIOUS WORK

The Flynn Creek feature was initially studied by Lusk (1927), Wilson and Born (1936), and Conrad et al. (1954; 1957). Lusk (1927) interpreted Flynn Creek as a giant sinkhole, whereas the others regarded the localized structural "disturbance" in the Flynn Creek area as a cryptoexplosion structure, but not of impact origin. In their classic review of several cryptoexplosion structures, Boon and Albritton (1936) synthesized evidence from Flynn Creek among other similar structures, all of which they envisioned as features of enigmatic explosive origin. Early researchers noted the profound difference in thickness of the Upper Devonian Chattanooga Shale inside versus outside the structure (up to a ten-fold increase in thickness within the crater, i.e., ~ 7 m outside the crater and up to 70 m inside the crater; Conant and Swanson, 1961). Wilson and Born (1936) were the first to remark that the Flynn Creek structure's age was likely to be pre-Chattanooga. They surmised that the Flynn Creek disturbance occurred sometime between Early Ordovician and Late Devonian, thus prior to the advance of the Chattanooga sea and upon the local erosional surface atop the Knox and other units. In an extensive stratigraphic analysis of the area, Conant and Swanson (1961) argued that the Flynn Creek structure formed sufficiently long before deposition of the Chattanooga Shale that it was eroded and filled with the breccia, which we regard today as being of impact origin.

During the late 1960s and 1970s, David J. Roddy and other U. S. Geological Survey geologists conducted extensive field work and core drilling at Flynn Creek (recounted in Hagerty et al., 2013; Gaither et al., 2015). From these field and core-drilling efforts, Roddy published a series of reports (including Roddy, 1966; 1968; 1977; 1979), which collectively established Flynn Creek as an impact structure mainly based on the overall distribution of structural features

within the structure, the structure-filling Flynn Creek impact breccia, minor ejecta preserved in a rim graben, and the presence of shatter cones in finely crystalline carbonate target strata.

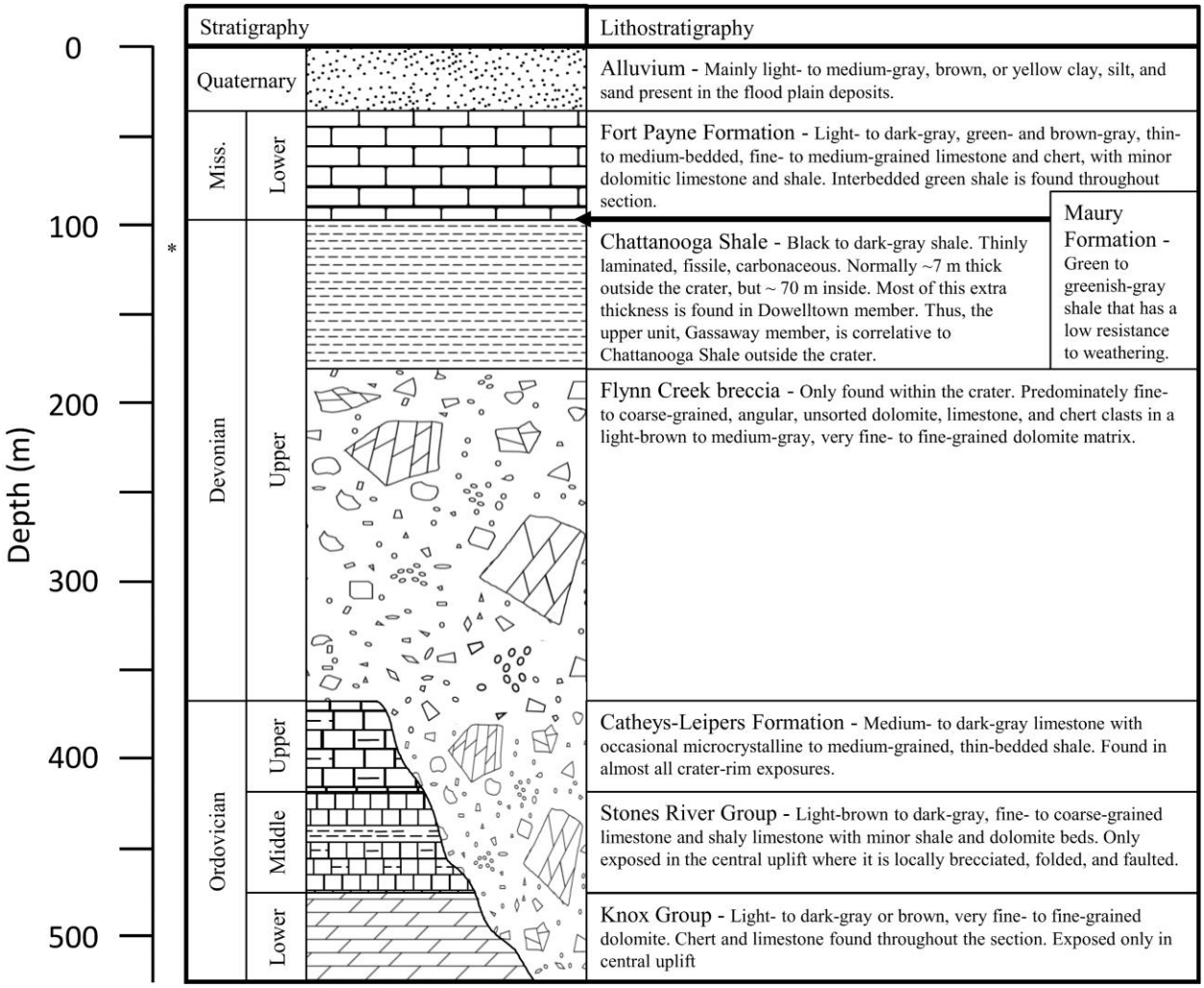

Figure 2. Target stratigraphic column for the Flynn Creek area. Descriptions of stratigraphic units and their thicknesses are given for each unit. Thicknesses are not to scale and the full thickness of the Knox Group is not shown. The cross-cutting relationship of the Flynn Creek breccia is schematic and the breccia does not extend to the Knox base. Arrow points to location of Maury Shale, less than 1 m thick. Modified from Conant and Swanson (1961), Evenick and Hatcher (2007), and other sources.

In his reports, Roddy (1966; 1968; 1977; 1979) interpreted the Flynn Creek impact structure as a Late Devonian, complex, marine-target impact crater, which had formed in a shallow, epicontinental shelf setting. However, Roddy stated the age of impact was some time

prior to Chattanooga Shale deposition, which means that the age of impact actually could be much older than Late Devonian as he suggested – perhaps even Silurian or Ordovician – based strictly on his observational data. Subsequently, based on coeval conodont elements recovered from the crater-filling impact breccias and an age analysis of those conodont elements based on extant radiometric age dating of conodont biozones in other places, Schieber and Over (2005) concluded that an age of ~ 382 m.y. (i.e., early Frasnian) was a reasonable stratigraphic estimate of the age of impact at Flynn Creek. Presently, this stratigraphic assessment may be the best age estimate for the Flynn Creek impact event.

Schieber and Over's (2005) conodont elements within the Flynn Creek resurge breccias likely came from an initial Chattanooga transgressive lag that formed early during the Chattanooga-related sea-level rise of Late Devonian. A basal Chattanooga lag or residuum deposit of less than 1 m situated between Chattanooga and underlying units from outside the impact structure proper was described in the study area by Conant and Swanson (1961). Schieber and Over (2005) suggested that the residuum was the likely source of conodont material that was washed back into the impact structure and thus mixed within the impact breccia. Schieber and Over (2005) also suggested very shallow marine water setting for the impact target, perhaps less than 10 m water depth, and if so, this early Chattanooga sea may not have had any appreciable shale accumulation at this early stage during transgression.

Schieber and Over (2005) studied some of Roddy's drill cores and described the post-impact transition from marine crater-filling breccias to the black shales of the Chattanooga. In this stratigraphic study, they described sequences of chaotic to bedded carbonate breccias in the moat of Flynn Creek impact structure. These sequences are similar in many aspects to the crater moat-filling breccia units at the marine-target impact structures Lockne and Tvären in Sweden

(cf. Ormö et al., 2007; 2010; and Sturkell et al., 2013). Like Roddy (1968), Schieber and Over (2005) recognized a basal non-bedded (or chaotic) breccia and an overlying bedded (or graded) breccia, which is a breccia dichotomy common to Lockne and Tvären (as reviewed by King et al., 2015; see also Azad et al., 2015).

The Flynn Creek breccia (or impact breccia) is an informal unit in the stratigraphy of the area. During U.S., Geological Survey investigations, Conant and Swanson (1961) and Roddy (1968) did not assign a formal lithostratigraphic status to the unit. Schieber and Over (2005) regarded the Flynn Creek breccia as the basal member of the Chattanooga Shale, and Evenick and Hatcher (2007) regarded the Flynn Creek as a separate stratigraphic unit of formation rank, but neither publication formalized this status.

OBJECTIVES

The present research examines the upper part of drill core FC77-1, which was drilled in 1977 to a total depth of 725 m into the western flank of the central peak of Flynn Creek impact structure (Fig. 1). Drill core FC77-1 is presently part of the Flynn Creek drill core collection at the U.S. Geological Survey Astrogeology Science Center in Flagstaff, Arizona. In this study, we describe the upper 175 m of the drill core, which represents the interval above the top of underlying broken and uplifted target formations (Stones River and Knox Groups) and below the present erosional surface of the central uplift. Thus, this interval encompasses the extant impact breccia lying upon the flank of the central uplift area of the impact structure. The overall objective of this study was to determine what the characteristics of these impact-derived sediments could tell us about impact processes in general at Flynn Creek and around the central uplift's flank in particular. We accomplished these objectives by combining grain-size analysis

using a modified line-logging technique and compositional analysis using line-logging and petrographic thin-sections.

METHODS

Sedimentological Analysis

Data regarding the clast sizes of various constituent lithologies in the central uplift breccias were collected in drill core FC77-1 from depths of 0 to 175 m by using the line-logging method described by Ormö et al. (2007; 2009). The line-logging method was chosen because it is a proven, non-destructive, fast, economic technique, and it is well suited for studying relatively long (> tens of meters) core sections of coarse-grained sedimentary rocks such as impact breccias. The results of line-logging in drill cores from within impact structures have produced tell-tale results with regard to sedimentary processes in relation to crater modification, notably at two impact structures in Sweden (Lockne and Tvären; Ormö et al., 2007; Sturkell et al., 2013), and the Chesapeake Bay impact structure, Virginia, USA (Ormö et al., 2009).

Line-logging is carried out by first delineating a thin line down the visible "center" of the core in the core box as viewed from above (Fig. 3a). This may be done by either stretching a thin sewing thread along the core or, as in this study, drawing a thin erasable line. The core is sprayed with water to more easily distinguish textural features such as clasts and matrix. Once the core is wet, every clast with a visible long-axis length equal to or larger than the pre-determined cut-off size (i.e., 5 mm in this study), which touches the line, is assigned a unique identifying number, then information about that clast number is recorded, including lithology, color, shape/roundness (per Powers, 1953), the depth in the core (as core box number and box slot number), and other information such as sedimentary structures or diagenetic alteration. In addition, note is made about whether the observed breccia texture in the vicinity of the clast is

clast- or matrix-supported (center column in Fig. 3b). Grain support is defined in this study as having a preponderance of grain-to-grain contacts that are evident on the drill-core surface and along the logging line. Clasts with a visible length less than 5 mm were excluded from line-logging analysis due to potential increase in measurement error and difficulty of consistently determining the clast lithology via hand lens, as well as the issue of it being more difficult to consistently discriminate small clasts from matrix (cf. Ormö et al., 2007; 2009; Sturkell et al., 2013). Bedding was not directly observed in the breccias, and thus not recorded by us, but some larger clasts contained relic original sedimentary bedding and that was used to delineate the margins of such clasts.

The method utilized herein provides grain-size frequency distributions with depth, and a plot of the occurrence of different clast lithologies and sizes throughout the studied interval of the drill core (0-175 m depth). We should note that core recovery was essentially one-hundred percent, and no unreported core losses were observed during our line-logging process. Therefore, there are no gaps in the sedimentological data over the 175 m span.

The line logging method as performed by Ormö et al. (2007; 2009) includes statistical analysis and data treatment. In this concept, clast size is first recorded in millimeters and then converted to phi (Φ) values following the formula:

$$\Phi = -\log_2 d,$$

where d is the grain diameter in millimeters (Folk, 1968).

Positive phi values (i.e., $-1*\Phi$) are used for convenience as well as to stay consistent with comparable data presented by Ormö et al. (2007; 2009) and Sturkell et al. (2013). Therefore, as our positive phi values increase, grain size will increase.

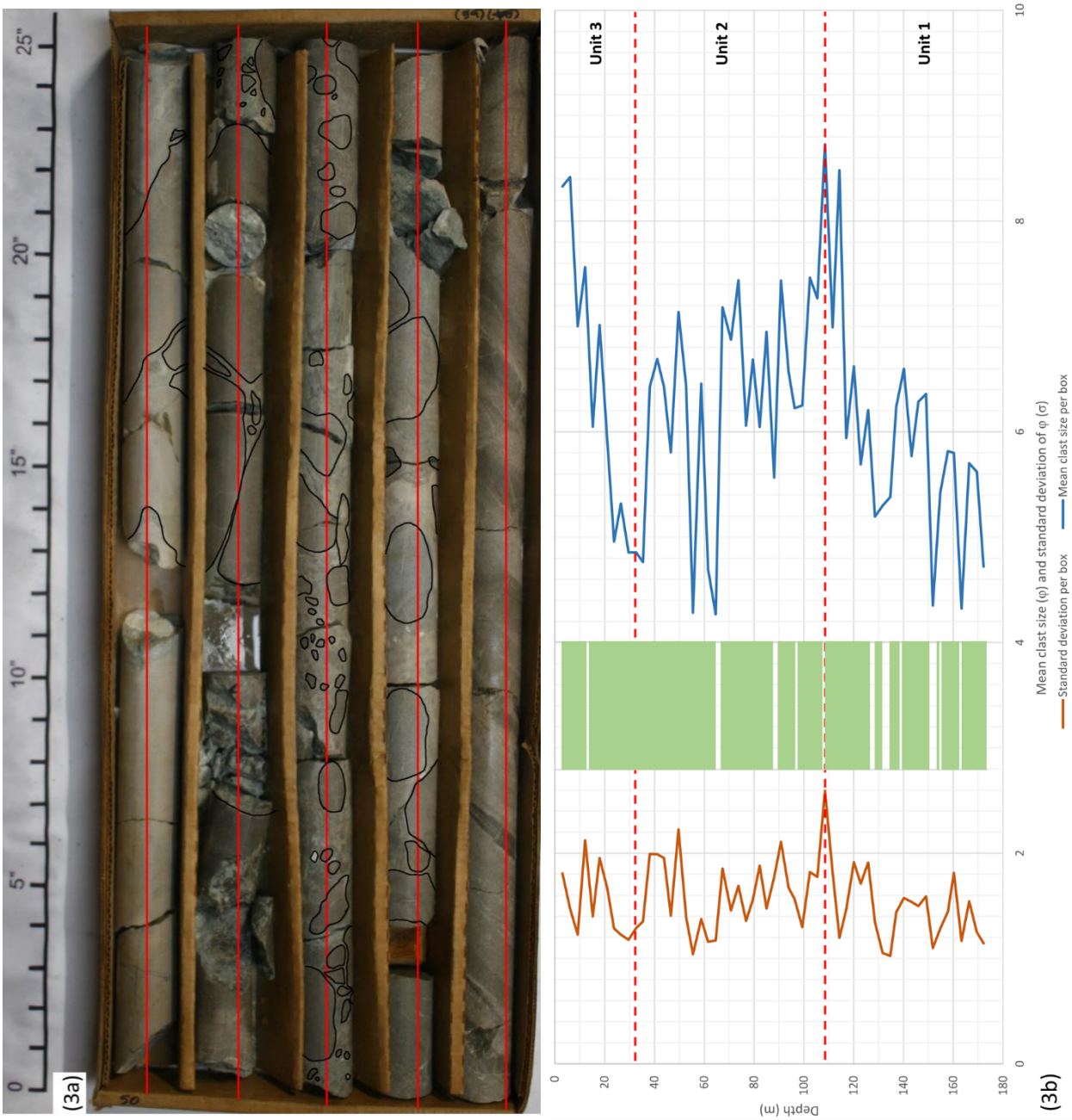

Figure 3. (a) Flynn Creek drill core FC77-1, core box number 45, which has been marked with a red line to simulate the location of a pencil line for the line-logging method. Clasts have been outlined in black on this image to show a typical arrangement of clasts (in this instance, a section of sedimentological unit 1). The length of each slot within the box is two English feet, or 61 cm. (b) Vertical (depth) plot of mean clast size per box (φ) on the right and standard deviation per box (σ_φ) on the left. The interpreted boundaries between sedimentological units 1, 2, and 3 are indicated. The vertical column between the clast size and standard deviation plots shows the vertical distribution of matrix support (white areas) and grain-support (green areas). Each horizontal line in this vertical column is one slot (61 cm) within a core box. Horizontal axis is arithmetic for both clast size and standard deviation.

Unlike Ormö et al. (2007; 2009) – who calculated the mean -Φ value per meter (φ) to analyze the clast-size variation and the standard deviation of φ (σ_φ) for every meter interval containing more than five clasts in order to analyze the size sorting – we used in in this instance more convenient depth intervals (i.e., the span of depth per box, which is ~ 3.05 m), but otherwise utilized the same analysis technique as Ormö et al. (2007; 2009; Fig. 3b). Boxes with fewer than five clasts in the box were not included.

Petrographic Analysis

The objective of thin-section analysis was to examine the nature of the breccia matrix and breccia constituent clast types. We made a total of 73 standard thin sections that span the interval from 0 to 175 m depth and more or less evenly represent all three sedimentological units. On average, there was one thin section per 2.4 m of FC77-1 drill core. Thin sections were examined using standard petrographic techniques and a description was made of the petrology of each thin section. Volume percentages of components were estimated using grain-density visual comparison charts and constituent minerals were identified petrographically, and in some instances supplemented by micro-FTIR and micro-Raman spectroscopy.

Regarding infrared spectroscopy, we collected micro-FTIR maps from one thin section using a Nicolet iN10MX FTIR microscope, in the Vibrational Spectroscopy Laboratory at Stony Brook University. This instrument is equipped with a liquid nitrogen-cooled HgCdTe array detector capable of acquiring hyperspectral image cubes between 715 and 7000 cm^{-1} (1.4-14 μm) at 25 μm/pixel spatial sampling.

Regarding micro-Raman spectroscopy, we collected micro-Raman spectra in the Vibrational Spectroscopy Laboratory at Stony Brook University using a WiTec alpha300R confocal imaging system, equipped with a 532 nm Nd YAG laser with 50 mW nominal power at

the sample surface, and a spot size of 0.76 μm. Each spectrum was acquired through a 50X (0.85 NA) objective, and consisted of 60 acquisitions each with a 1-second integration time.

RESULTS

Sedimentological Analysis

The plot of the vertical distribution of mean -Φ values per box (φ) and standard deviations (σ_φ) per box versus depth revealed that there are three distinctive sedimentological units (numbered 1 through 3 in Fig. 3b) within the 175 m-thick impact breccia unit in the FC77-1 drill core. Sedimentological unit 1 displays an overall coarsening-upward sequence from approximately 4.7 φ to a terminal peak of approximately 8.7 φ, which spans the interval from 175 to approximately 109 m. The coarsening-upward is not continuous; it has a 'saw-tooth' pattern of the grain sizes expressed as shifts in φ values throughout the interval. Unit 1 also displays standard deviation (i.e., size sorting σ_φ) values ranging from approximately 1.2 to approximately 2.5. In unit 1, this standard deviation plot also shows a 'saw-tooth' pattern similar to that of φ values. The peak value of 2.5 in σ_φ coincides with the grain-size peak (~ 8.7 φ, and thus marks the top of sedimentological unit 1. Hence, the top of unit 1 is coarser and more poorly sorted than the lower part of the unit.

Sedimentological unit 2 displays an overall fining-upward sequence from approximately 8.7 φ to a terminal low of approximately 4.7 φ, which spans approximately 109 to 32 m in depth (Fig. 3b). The fining upward is not continuous; it has a 'saw-tooth' pattern that is generally similar to what was noted within unit 1. Unit 2 similarly displays σ_φ values (i.e., size sorting) ranging from approximately 2.5 to approximately 1.2. This standard deviation plot also shows the same 'saw-tooth' pattern of the σ_φ values versus depth as for unit 1 (Fig. 3b). The value of 2.5 σ_φ at the top of the unit coincides with the grain-size low of approximately 4.7 φ. Thus, it is

evident that the top of sedimentological unit 2 is more fine-grained and better sorted than the lower part of the unit.

Sedimentological unit 3 displays a truncated coarsening-upward sequence that peaks at approximately 8.4 φ near the top of the drill core. Standard deviation shifts between about 1.2 and 2.2. The top of unit 3 is zero meters in the FC77-1 drill core, which is an erosional surface at ground level, and its base is approximately at 32 m. Grain support increases over the span of unit 3.

Figure 4 shows the distribution of our 2076 individually measured clasts (color-coded according to lithology) on an arithmetic vertical scale and a logarithmic horizontal size scale (in mm). Regardless of size, the vast majority of clasts are dolomitic (blue dots). Unit 1, ranging from 175 to approximately 109 m, contains a higher percentage of limestone clasts, but only over the lower 20 m. Above that level, mainly dolostone clasts prevail. Some chert clasts occur at approximately the level where limestone diminishes in favor of dolostone (~ 154 m) and chert clasts again appear within +/- 5 m of the 130 m level. A few "other" clasts, mainly shale, occur in the middle part of the unit. Unit 2, ranging from approximately 109 to 32 m, is dominated almost exclusively by dolostone clasts. Near the base of unit 2, some "other" (mainly shale) clasts appear, and some chert clasts occur around depths of 84 and 46 meters. Unit 3 is dominated by dolostone clasts, but a few limestone clasts occur mainly in the upper few meters of the unit.

Petrographic Analysis

Overall, the Flynn Creek breccia in the upper 175 m of the FC77-1 drill core is a carbonate breccia composed mainly of fine- to medium-sized clasts. The clasts themselves consist mainly of grey dolostone clasts (plus a minor component of other kinds of clasts and

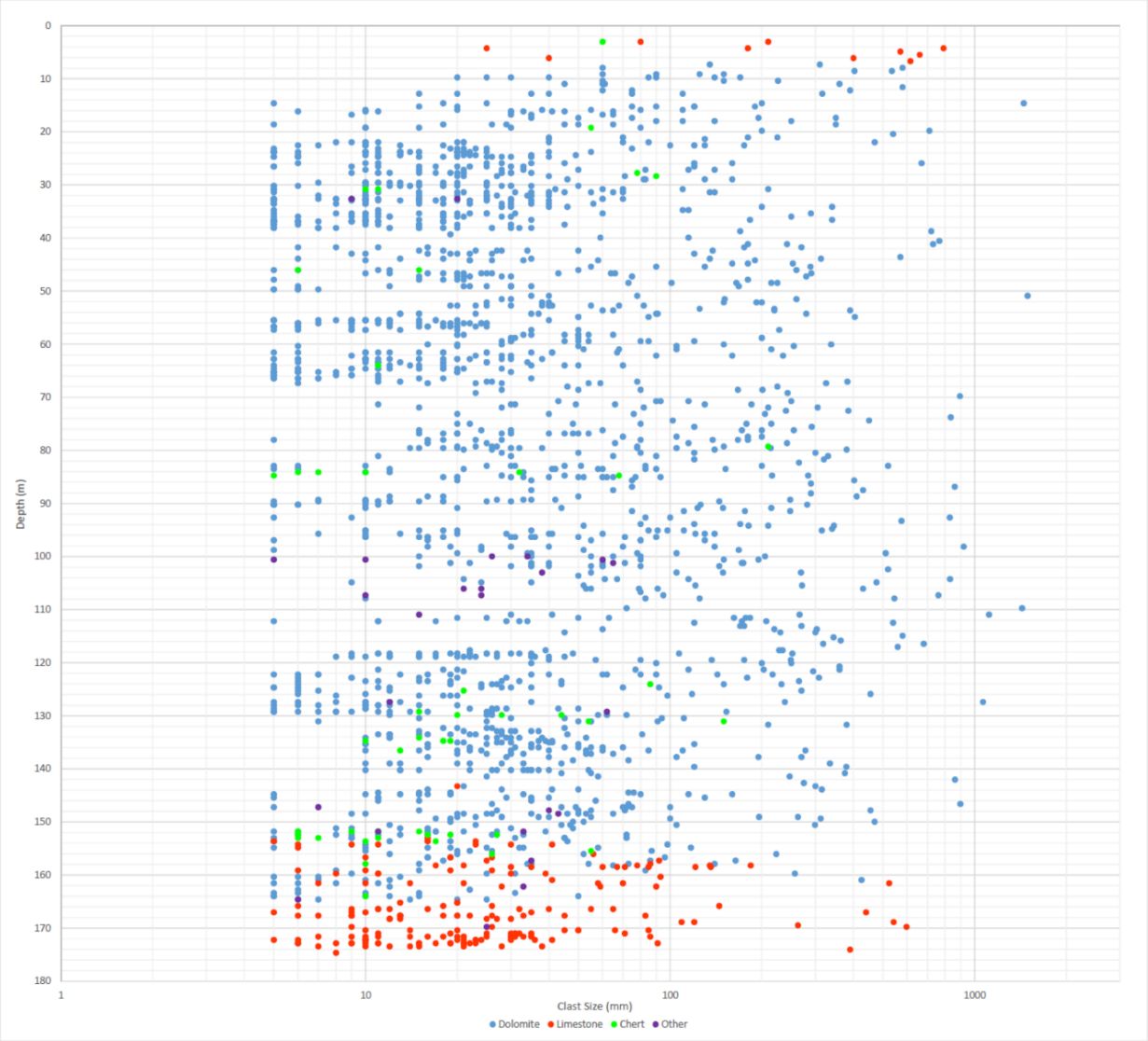

Figure 4. Vertical (depth) plot of individual clast size measurements. Each dot (N=2076) represents a single clast recorded from line-logging that has been color-coded according to lithology; dolostone is blue, limestone is red, chert is green, and other clasts are purple. Dolostone is by far the most common clast type in the logged interval, which stands to reason considering that the main target layer was the Upper Ordovician Knox Group, a thick dolostone unit, and that the target units above the Knox are mainly carbonates as well. Chert, which is less abundant than dolostone but still widely distributed like it, likely also came from beds within the Knox or younger carbonate units where chert is common. Limestone was primarily logged within two intervals; the upper 10 meters and lower 20 meters of logging.

clastic grains, i.e., less than 10 percent). These clasts and grains occur within a grey to grey-brown matrix of fine-grained dolostone, limestone, chert, minor amounts of dark clay, and traces

of opaque materials including some pyrite. The overall matrix content was about 25 percent for the whole of the 175-m interval studied.

As shown in Figure 4, based on megascopic core description, the sizes of clasts in this breccia range from approximately 5 mm to 1.6 m, but most observed clasts are in the range of 5 to 130 mm. Five millimeters was the cut-off lower size limit in our visual core descriptions. Therefore, the finer clasts (especially those under 5 mm in long dimension) were examined in detail in the petrographic thin sections. These < 5 mm clasts, which occur in the matrix between larger clasts, generally consist of (in order of abundance): (1) fine to medium dolostone (75%: Figs. 5a, b); (2) coarse dolostone fragments or large dolomite crystals (10%); (3) finely crystalline chert (5%); (4) fine fossiliferous and/or oölitic limestone and/or dolostone (4%); (5) cryptocrystalline melt clasts (4%; Figs. 5c-f and 6a, b); (6) rounded and sub-rounded fine to medium quartz grains and sub-rounded feldspar grains of similar size to the quartz (<1%); and (7) rounded, laminated brown shale clasts (<1%). Overall, dolostones comprise about 90 percent of the larger clasts and 89 percent of the <5 mm clasts in the samples examined (i.e., fine to medium dolostone, coarse dolostone fragments or large dolomite crystals, and fine fossiliferous and/or oölitic limestone and/or dolostone). Dolomitization of target strata is interpreted to have been a pre-impact process, as noted by Roddy (1968) and others.

Petrographically, the <5 mm, fine to medium dolostone fragments and coarse dolostone fragments are generally very similar in petrographic characteristics to the larger dolostone clasts (i.e., 5 mm–1.6 m grain sizes), some of which were also studied in thin section. All of these dolostones are sparsely fossiliferous and usually contain a small component of dolomitized fossil fragments, pellets, and rare oölites. The dolomitization process in the target rocks was not pervasive, thus allochemical grains can be seen preserved at least in part within the texture of the

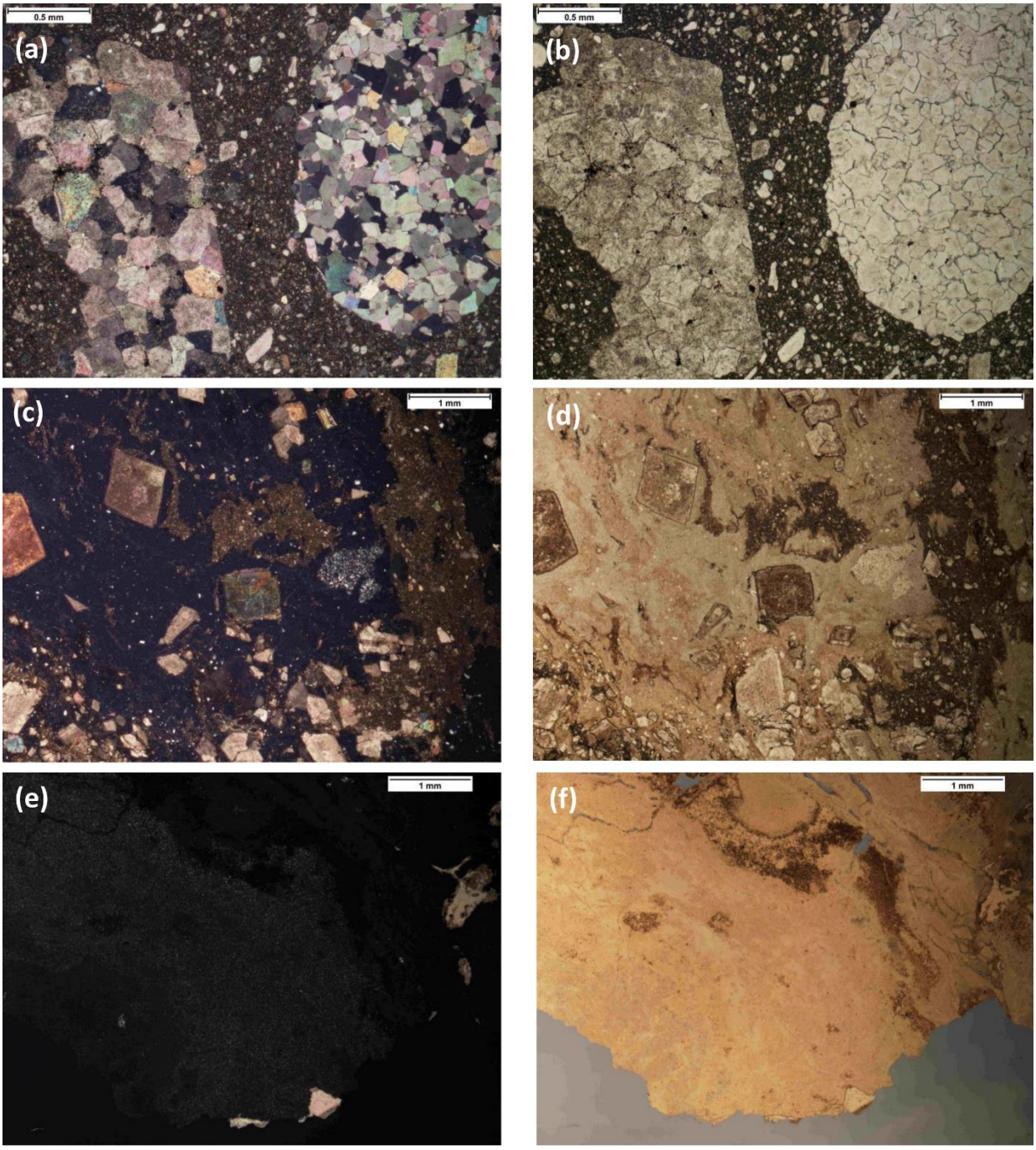

Figure 5. (a) Photomicrograph of dolostone clasts having medium crystallinity within a finer dolomitic matrix that includes fine dolostone fragments and clastic (quartz and feldspar) grains. Scale bar (0.5 mm) is given on each image. Cross-polarized view. (b) Same as (a), but plane light. Sample FC77-1-57-B. (c) Photomicrograph of cryptocrystalline melt with flow features and inclusions, including dolostone grains, chert fragments, and dolomite crystals. Cross-polarized view. (d) Same as (c), but plane light. Sample FC77-1-45-B. (e) Photomicrograph of cryptocrystalline melt with flow features and dolomitic inclusions. Cross-polarized view. (f) Same as (e), but plane light. Sample FC77-1-29-A.

constituent dolomite crystals. Identifiable, fossil fragments include trilobites, brachiopods, mollusks, bivalves, and echinoderms. Fossiliferous and/or oölitic limestone and/or dolostone are far less common than other carbonate grains in the breccia matrix. Besides having a finer crystallinity, these grains are overall very similar to the more coarsely grained dolostone clasts. Dolomite crystal inclusions in the breccia matrix consist of large to medium euhedral dolomite crystals and masses of several euhedral dolomite crystals up to 1 mm across. Some of these dolomite crystals and crystal masses contain closely spaced planar fractures and associated darkening of the crystals in the vicinity of the fractures. These closely spaced fractures look very much like planar deformation features in quartz as described by many other workers as indicators of shock deformation, and these dolomite features have been noted by Roddy (1968) as possible effects of the impact. However, we do not view them as such because carbonate minerals can easily develop features such as closely spaced twin lines, during many stress events of handling (drilling, cutting of core, thin-section making, etc.). The larger dolomite crystals seem to be particularly susceptible to these closely spaced twin lines.

Finely crystalline chert clasts range in size from medium sand (0.25 mm) to fine gravel (5 mm). In some instances, these fragments exhibit patches of chalcedony within them or along their margins. Even though these chert clasts are finely crystalline, the individual quartz and chalcedony crystals are easily discernible within the chert grains even at low power magnification, and no chert grains observed had crystals so fine that the texture appeared glassy. Some of these small chert grains contain relic oölites, pellets, and fossil fragments. The chert fragments' inclusion suite mimics the dolostone suite, supporting the notion that these chert fragments are from early-formed cherts that replaced the carbonate materials in the target dolostone formations prior to impact.

Cryptocrystalline melt clasts, which have not been reported previously at Flynn Creek impact structure, include 1-5 cm, irregular to subrounded masses of extremely fine-grained quartz. In cross-polarized light, the melt clasts appear to be isotropic, except for a few fine- to medium-sized dolomite crystal inclusions. However, micro-FTIR and micro-Raman spectroscopic analysis reveals that the melt clasts are in fact made of crystalline quartz. The crystal size is likely significantly less than the thickness of the sample on the thin section, or < 30 μm.

Micro-FTIR spectroscopy indicates two phases: dolomite clasts within a quartz matrix (Fig. 6c-f). The dolomite exhibits characteristic peaks centered at 1527 cm^{-1}, 1095 cm^{-1}, and 894 cm^{-1}. The quartz matrix exhibits a strong peak at 1080 cm^{-1} and smaller peaks at 1172 cm^{-1} and 902 cm^{-1}. Micro-Raman spectra taken from within the matrix show it is dominated by quartz, with characteristic Raman peaks at 464 Δcm^{-1}, 206 Δcm^{-1}, and 128 Δcm^{-1} (Fig. 6g). Despite the clasts being nearly optically isotropic, micro-FTIR and micro-Raman spectroscopy indicate that the clast matrix is crystalline. The clast matrix exhibits strong infrared peaks at 1080 cm^{-1} and 1172 cm^{-1} consistent with SiO_2 phases.

In effect, the crystal size is so minute in the cryptocrystalline melt that even though the optical behavior overall mimics glass, the crystal structure is intact at a very small scale. In plane light, cryptocrystalline melt clasts are clear, pinkish, greenish, or brownish and they contain wavy bands and unique inclusions. These characteristics contrast with chert grains present in the breccia matrix, which do not have the colors and crystallinity of the cryptocrystalline melt clasts. Most cryptocrystalline melt clasts display a suite of inclusions that differ from the inclusions within the chert fragments in that the melt clasts inclusions look like

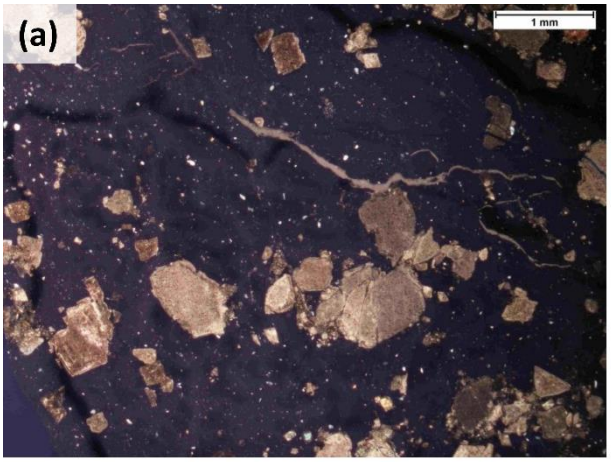
(a)
1 mm

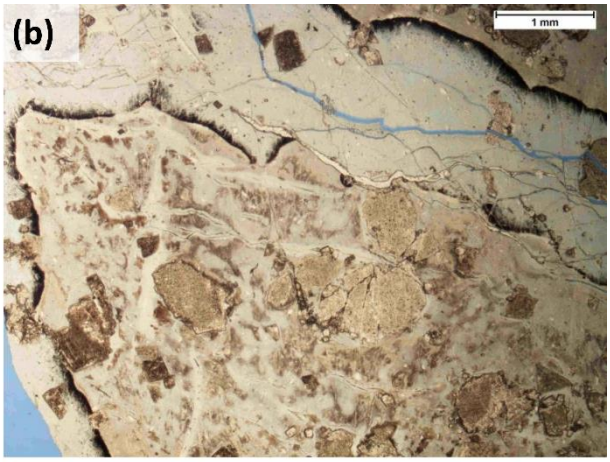
(b)
1 mm

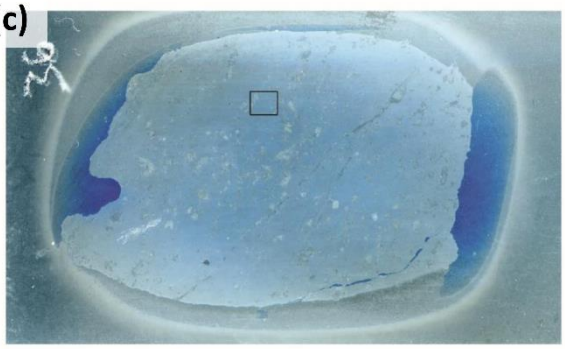
(c)

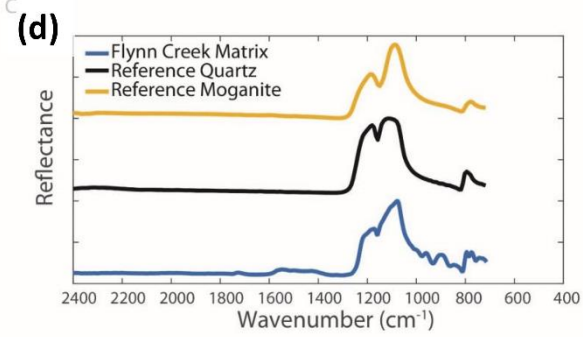
(d)
Flynn Creek Matrix
Reference Quartz
Reference Moganite
Reflectance
2400 2200 2000 1800 1600 1400 1200 1000 800 600 400
Wavenumber (cm-1)

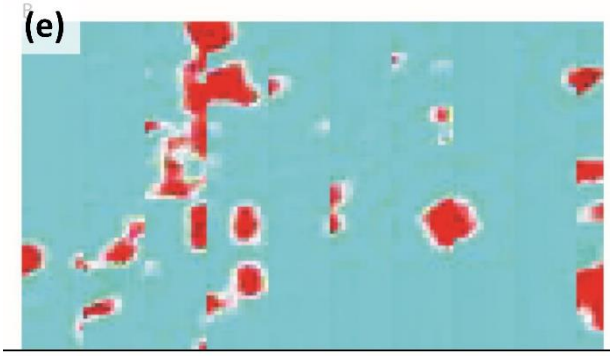
(e)

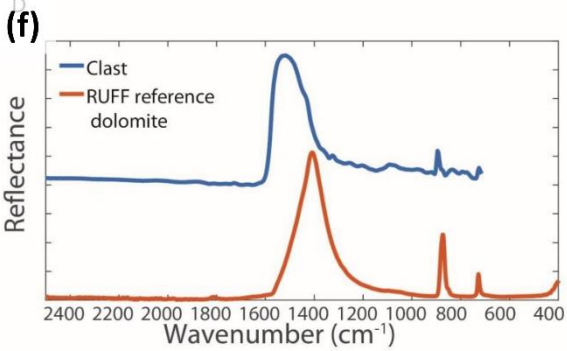
(f)
Clast
RUFF reference
dolomite
Reflectance
2400 2200 2000 1800 1600 1400 1200 1000 800 600 400
Wavenumber (cm-1)

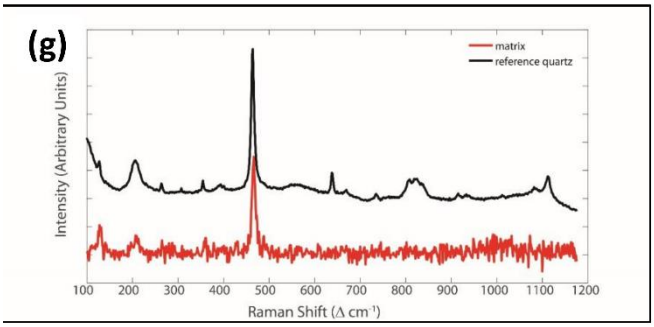
(g)
matrix
reference quartz
Intensity (Arbitrary Units)
100 200 300 400 500 600 700 800 900 1000 1100 1200
Raman Shift (Δ cm-1)

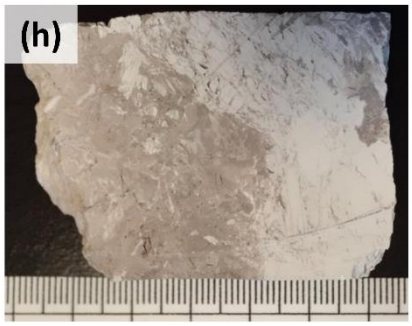
(h)

Figure 6. (a) Photomicrograph of cryptocrystalline melt with flow features and dolomitic inclusions. Cross-polarized view. (b) Same as (a), but plane light. Sample FC77-1-45-D. (c-f) Micro-FTIR image, map, and spectra related to melt in thin section FC-77-1-45-D. (c) Scanned image of the thin section showing the location of the micro-FTIR map (box). Map is 3.5 x 2 mm. (d) IR map displaying the primary dolomite peak (1525 cm^{-1}) in red and quartz peak (1084 cm^{-1}) in blue. (e) Micro-FTIR spectra of the matrix and reference quartz and moganite from Hargrove and Rogers (2013). (f) Micro-FTIR spectra of the dolomite clast and reference dolomite (from RUFF database). (g) Micro-Raman spectra of the matrix and reference quartz. The matrix exhibits only the characteristic peaks for quartz (at 464 Δcm^{-1}, 206 Δcm^{-1}, and 128 Δcm^{-1}) and not the 501 Δcm^{-1} peak diagnostic of moganite. From sample FC77-1-45D. (h) Drill-core sample slice showing cryptocrystalline melt (light grey on the right) and dolomitic impact breccia matrix on the right. Scale bar is in centimeters; small ticks are millimeters. Sample FC77-1-28-A.

clasts such as those derived from target carbonates, and other components such as dolomite crystals, chert fragments, and quartz grains.

Melt clasts are rare enough that they only were found very infrequently during logging line, and when they did, we counted them among the "other" clasts in compiling the data for Figure 3b. It was not until subsequent thin-section analysis that these phases were determined to be in fact melt clasts. We found them generally throughout the lowermost sedimentological unit (unit 1) and the lower 20 m of sedimentological unit 2, but not elsewhere in the 175-m thick section studied. On the cut face of samples selected for thin-section making, the melt clasts are generally much lighter than the adjacent rock, usually white or light grey, and have highly irregular margins in contact with the enclosing grey to grey-brown breccia matrix (Fig. 6h).

Melt in any form has not been previously noted at Flynn Creek and is rare in carbonate-target impact structures in general (Osinski et al., 2008). Melt in carbonate-target impacts can have complex mineralogy and may include melt of carbonate minerals (Osinski et al., 2008). However, at Flynn Creek, the melt we found is interpreted to have been originally silica, which is now cryptocrystalline quartz. We should note that a previous suggestion that some Flynn Creek materials may have been melted was made by Evenick et al. (2004), with regard to

possible melt within or along stylolites. Typically, stylolites are pressure-solution features that are abundant at junctures in the rock where carbonate textures change abruptly.

Stylolites were a common feature in our thin sections from FC77-1. Because of their close association with original bedding contacts (and thus original textural changes in carbonate lithology), stylolites are shown to be mainly pre-impact features of the target section. Rare stylolites appear to have developed along the margins of some dolostone clasts within the impact breccia, owing to post-impact compaction, but still not considered an impact melt feature either.

Framework silicates, i.e., quartz and feldspar, comprise only a very small percent of the breccia matrix. The average quartz grain in the breccia matrix is slightly more rounded than the average feldspar grain (i.e., subrounded versus subangular), but the sizes of the two are about the same on average (i.e., fine to medium sand). The quartz grains mainly appear to be recycled grains of original granitic origin, which is indicated by curviplanar trails of inclusions and regular jig-saw domains within multi-crystalline grains. Feldspars are not highly altered, and there was no observed maskelynite; in most feldspars, twinning is common. Approximately 10 percent of quartz grains display widely spaced or roughly orthogonal planar fractures, but there were no observed planar deformation features (PDFs), feather features (FFs), or other impact-related effects like toasting or partial melting.

DISCUSSION

Sedimentological Analysis

Sedimentological analysis of marine target impact structures has been reported in a relatively small number of impact structures. These impact structures include Manson (Witzke and Anderson, 1996), Chesapeake Bay (Gohn et al., 2005; Ormö et al., 2009), Gardnos (Kalleson et al., 2008), Lockne and Tvären (Ormö et al., 2007; Sturkell et al., 2013), Kärdla (Puura and

Suuroja, 1992), and Ritland (Azad et al., 2015). We here choose to compare our results of the Flynn Creek core analysis with those presented for the Locke and Tvären impact structures because of (1) the applied methodology in the sedimentological analysis, (2) their sizes (Lockne, 7.5 km, and Tvären, 2 km, versus Flynn Creek, 3.8 km), and (3) their predominantly carbonate target strata. However, the difference between our work and that on Lockne and Tvären (Ormö et al., 2007; Sturkell et al., 2013) is that their work was done on breccia moat deposits, whereas the present study focuses on the flank of the central uplift.

The sedimentary characteristics of Flynn Creek's unit 1 in the FC77-1 drill core show both differences and similarities with to those at Lockne and Tvären crater-filling breccias. Work by Sturkell et al. (2013) on the Tramsta Breccia at Lockne, which was formed by slumps from the crater rim, showed the transition from this underlying slump-derived breccia to the overlying resurge breccia (i.e., the Lockne Breccia). In the poorly sorted and coarser slump-derived Tramsta Breccia, there is a 'saw tooth' pattern in the size-sorting graph, but this is less evident in the resurge breccia where grain sizes are much finer and sorting is much better. There are coarsening-upward trends in some sub-sections of the Tramsta slump-derived breccia, though it lacks a general coarsening-upward trend over the entire unit (Sturkell et al., 2013). By contrast, resurge breccias at Lockne and Tvären have a distinctive, general fining-upward trend, as documented by Ormö et al. (2007). A review of marine impact sedimentology by Azad et al. (2015) shows that sedimentary moat breccia sequences in several marine impacts, including Ritland in Norway, do not compare with sedimentary characteristics that we observed in drill core FC77-1 on the flank of the Flynn Creek central uplift, and we did not expect that there would be a good comparison given the difference of location.

The coarser grain size, poorer sorting, and evident coarsening-upward trend in Flynn Creek's sedimentological unit 1 suggest that it formed by a different mechanism than the slumping of the Tramsta Breccia. The slumps forming the Tramsta Breccia were strongly influenced by a large amount of unconsolidated, black mud (i.e., the Alum Shale). Instead, the mechanism for Flynn Creek's unit 1 seems more similar – to or closely akin to – debris or rock avalanches, likely emanating from the rising central peak, wherein an overall larger clast size and coarsening-upward textures might be expected. Studies of modern debris and rock avalanches, and the transition realm between those two mass-movement processes (i.e., debris and rock), document the coarse grain sizes, poor size sorting, and coarsening-upward trends seemingly akin to unit 1's characteristics (see modern studies by Shreve, 1968; Hungr, 1990; Hungr and Evans, 2004). The central uplift is the most likely source for the debris in unit 1 because it is the most proximal source. An alternative rim source is considered very unlikely to impossible because of the substantial distance away (approximately 1.5 km to the rim from the drill hole site).

In particular, the process of generating a 'saw tooth' coarsening-upward, grain-size and sorting pattern may result from successive emplacements of moving masses of debris or rock fragments from an upper slope area, wherein movements of debris and/or moving rock masses that are fragmenting as they go collide with a finer grained mass already in place at lower elevation. The moving mass of debris or rock fragments then experiences mass loading and partial substrate entrainment of fines already in place. We suggest that this could be a viable mechanism for production of the progressively coarsening-upward steps within the overall coarsening-upward trend within Flynn Creek's unit 1 (see especially the discussion of momentum transfer in Hungr and Evans, 2004). The center column in Figure 3b also shows that

there are intervals of matrix support, especially within unit 1, which may relate to finer intervals already in place as in the momentum transfer process.

Figure 7 is a model for the emplacement of a single coarsening-upward section within sedimentological unit 1, as styled after the momentum transfer process of Hungr and Evans (2004). As debris or rock material moves downward along the flanks of the central uplift, i.e., through time-steps T_1, T_2, T_3, and T_4, that material interacts with and comes to reside upon the finer deposits already in a lower potential energy position (at time step T_4; Hungr and Evans, 2004). Successive, progressively coarser emplacement events likely built up the overall coarsening-upward package that is unit 1.

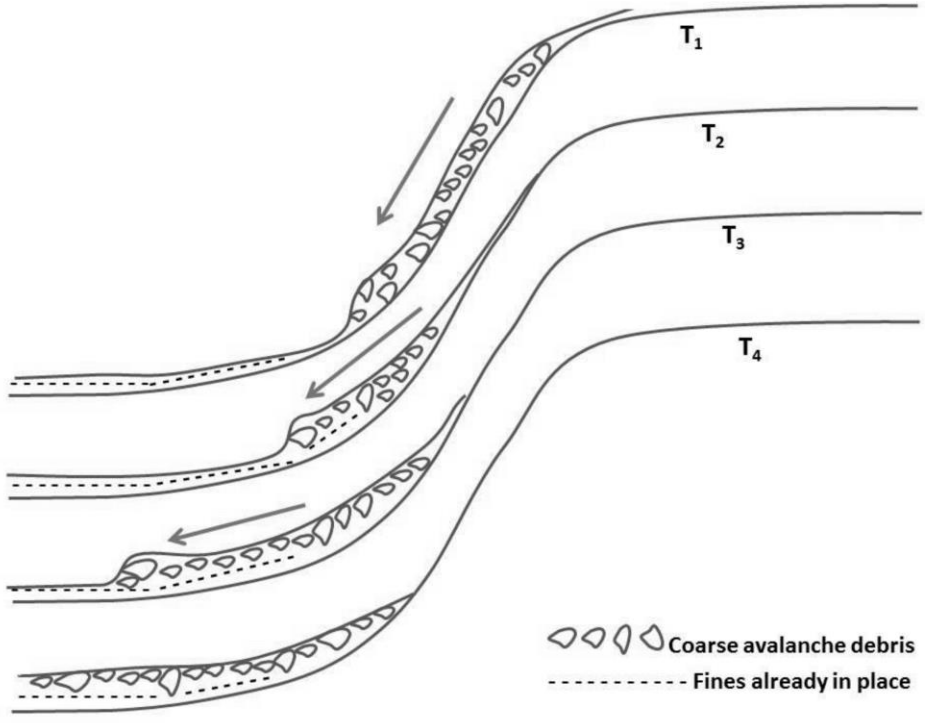

Figure 7. Depositional model for development of coarsening-upward deposits within sedimentological unit 1 of Flynn Creek impact structure's drill core FC77-1. Slope depicts a flank of the central uplift. T_1, initiation of debris or rock avalanche from the central uplift. T_2, downslope movement begins to interact with finer deposits already in place at the base of slope. T_3, debris or rock materials engage in momentum transfer in which they partially mix with and entrain fines. T_4, a coarsening-upward unit is produced by the mass-movement process. Modified from Hungr and Evans (2004).

Marine resurge waters, or waters seeping through fractured target units, were likely already filling the Flynn Creek impact structure, therefore we envision the avalanche process as likely occurring, or terminating, in an aqueous setting.

The sedimentary characteristics of Flynn Creek's unit 2 in the FC77-1 drill core also are dissimilar to the resurge units at Lockne and Tvären even though both possess overall fining-upward trends and the tendency toward better sorting near the top (cf. Ormö et al., 2007; Sturkell et al., 2013). Some of these differences are likely due to the fact that the Lockne and Tvären drill cores were taken in the moat breccia area and FC77-1 is on the flank of the central uplift; though it is feasible to expect other processes to have occurred as well. Flynn Creek's unit 2 is more coarsely grained, contains much less matrix supported material, and is overall more poorly sorted than resurge breccias at Lockne and Tvären. Within these two impact structures, grain sizes (φ) ranged from approximately 2 to 4 φ and sorting (σ_φ) ranged from approximately 0.1 to 1.87 (Ormö et al., 2007). In contrast, the φ values at Flynn Creek are approximately 4.7 to 8.7 and σ_φ ranges approximately from 1 to 2.5. At Lockne and Tvären, some parts of the resurge deposits are interpreted to be closely associated with the collapse of the central water plume, which caused a momentary "dumping" of more poorly sorted material, as well as a subsequent increase in water velocity causing a reverse grading (Ormö et al., 2007). We do not suggest, however, that a similar plume-collapse process had anything to do with the emplacement of unit 2 at Flynn Creek, which has a distinctive, overall fining-upward size distribution, but is also relatively very coarse overall (as compared to Lockne) and contains strong shifts in grains size and sorting (i.e., the 'saw tooth' pattern).

It is known from the Lockne Breccia, in locations mainly outside the Lockne crater, that the breccia may have a lower, poorly sorted and matrix-rich section, which is interpreted as

being moved by traction driven by an over-riding suspension flow (von Dalwigk and Ormö, 2001; Lindström et al., 2005). If Flynn Creek's unit 2 formed by such material movements, this would require that deposits from any suspension flow (driving the transport of unit 2) either existed on the flank of the central uplift, or elsewhere within the crater. Nevertheless, we favor an interpretation for unit 2 that it formed by debris flows coming down from the central uplift, which entered standing water on the flank of the central uplift. This material may have been sorted and graded by turbiditic settling (according to Stokes' Law) in the water column. In some instances, debris flows may have mixed with finer materials that were transported earlier by resurge flows or other processes bringing marine water over or through the rim and the then-extant proximal ejecta blanket. This mixing may have produced the coarser textures observed in fining-upward segments within the overall fining-upward sequence characterizing unit 2.

Previous work suggested very shallow water conditions at Flynn Creek, perhaps as shallow as 10 m water depths (Schieber and Over, 2005). If this was so, resurge may have been slower, and less energetic, than resurge at Lockne impact structure (i.e., 500 m target water depth), for example. This may mean that resurge had little if any influence on the deposition of Flynn Creek's unit 2. Nevertheless, it is also possible that marine resurge was finished by the time that sedimentological unit 2 at Flynn Creek was deposited, and implying a sedimentation by turbiditic flow into standing water (hence the observed fining-upward segments and overall fining-upward sequence). Settling in water would contribute to the overall better sorting and the fining-upward patterns of unit 2.

The sedimentary characteristics of Flynn Creek's unit 3 are similar to its unit 1, and thus may represent a return to dominant debris or rock avalanche processes of sedimentation, as discussed earlier. Even though the grain size and sorting patterns are similar to unit 1, the

presence of matrix support is essentially nil (Fig. 3b), which may relate to unit 3's higher position in the flank-related sequence (fines tend to accumulate more at the base of the flank, assuming the model for unit 1 is approximately correct). Unit 3 is truncated by an erosional surface (that is also the present ground surface), therefore we do not have a complete record of unit 3 in the FC77-1 drill core, thus making an interpretation of unit 3's origin somewhat more difficult.

Petrographic Analysis

The target section is strongly dominated by dolostone units (see lithology notes in Fig. 2), and thus a plethora of dolostone clasts is to be expected. Approximately 90 percent of all clasts in the Flynn Creek impact breccia are dolostones. None of the formations has highly distinctive fossil fauna that can help identify the source for lithic clasts and the extent of dolomitization is not helpful as a diagnostic indicator of provenance formation. Nearly all the carbonate target units have some small amounts of chert and sand layers within them, making the presence of such material non-diagnostic to their specific origin. Therefore, our petrographic analysis was not able to distinguish the provenance formation for most of the clast types. Only the Maury Formation, which is a shale unit approximately 1 m thick in the target area, has a lithology that is distinct enough to identify in small fragments (light brown shale with quartz silt and micas). We think that the Maury is the origin of the < 1 percent shale clasts in the impact breccia matrix (i.e., the distinctively black, silt-free Chattanooga Shale proper is not thought to have been a target unit, as noted in other comments above).

Hargrove and Rogers (2013) measured micro-FTIR spectra of quartz- and moganite-bearing rocks and suggested that subtle differences between the infrared spectra of quartz and moganite can be observed. For example, the ratio of the 1095 cm^{-1} and 1157 cm^{-1} peaks is

slightly different between the two phases (Fig 6c-f). Hargrove and Rogers (2013) also showed that these phases can be distinguished with micro-Raman spectroscopy, where moganite exhibits an additional peak at 501 Δcm^{-1}.

Based on the micro-Raman spectral peak positions of 464 Δcm^{-1}, 206 Δcm^{-1}, and 128 Δcm^{-1}, and a lack of the 501 Δcm^{-1} peak, we have interpreted the matrix of the Flynn Creek cryptocrystalline melt clasts to be composed of quartz (Fig. 6g). Micro-FTIR spectra are less straightforward to interpret. The micro-FTIR spectrum – taken in the same location as the micro-Raman spectrum – is a better match for the spectrum of moganite from Hargrove and Rogers (2013). The position of the primary peak at 1095 cm^{-1} is offset from the quartz peak, and the intensity of the 1157 cm^{-1} peak is lower than in the reference quartz. However, Hargrove and Rogers (2013) did not address potential changes in the infrared spectrum – specifically in terms of peak positions and intensities. We suggest that these differences could be the result of a different orientation of our sample from those measured by Hargrove and Rogers (2013), because shifting by ~10 wavenumbers and changes in intensities of peaks are common orientation effects in silicates. Therefore, our best interpretation for the melt clasts is quartz, based on a combination of the micro-FTIR and micro-Raman results.

Cryptocrystalline melt clasts are interpreted to have formed by melting of minor silica-rich components in the target. We think that the melt did not cool rapidly enough for silica glass to have formed, and therefore the melt cooled just slowly enough so that a very finely crystalline quartz texture emerged. The lack of carbonate melt at Flynn Creek is also important to note. One possibility for the dearth of carbonate melts is that these rocks never experienced temperatures high enough to melt the target carbonates, or if they did, vaporization occurred. Melting of quartz also requires extremely high temperatures, but given the abundance of chert in

the target rocks, the SiO_2 melt clasts may have originated from melting of this constituent chert. Incorporation of water in chert is common, and would significantly lower the melting temperature, thus allowing for SiO_2 melts, but perhaps not carbonate melts. In any event, the presence of these rare siliceous melt particles shows that melt formed in this impact event and can be preserved, albeit in a non-glassy cryptocrystalline form.

Micro-FTIR spectra of the clasts within the melt show strong peaks at 1572 cm^{-1} and 975 cm^{-1} consistent with dolomite (Fig. 6c-f). As with the quartz, there is slight difference in peak position, which we attribute to either orientation differences between the reference and this sample or slight differences in specific Mg and Ca abundances. Interestingly, the peak at 1572 cm^{-1} is slightly broader than is typical for dolomite, which may suggest some minor (thermal?) distortion of the lattice. Infrared spectroscopy, however, is not diagnostic for identifying shock effects in carbonates, and thus, we cannot uniquely attribute these features to impact effects.

At Lockne impact structure, minute melt fragments have been noted to make up a significant part (as much as 20% in some locations) of the fine-grained part of the resurge deposits at the Lockne impact structure (first noted by Simon (1987) and shown to be impact melt by Sturkell (1998)). In a water-rich target environment, such as a marine-target impact structure, the formation of melt may be more explosive causing a relatively higher volume of fall-back melt particles than melt pooling within the crater (e.g., Kieffer and Simonds, 1980; Ormö and Lindström, 2000). The subsequent resurge flow may cause an additional disintegration of the melt fragments as well as an accumulation of the particles within the fine-grained parts of resurge deposits, as suggested at Lockne. Hence, their volumetric rarity and small particle size at Flynn Creek.

We regard the cryptocrystalline melt clasts, which we found in the breccia matrix of FC77-1 drill-core samples, as the second line of definitive evidence, after shatter cones, for the impact origin of the Flynn Creek impact structure. We suggest that the minor quartz and/or chert components within the target stratigraphy may have contributed to the development of a small amount of silica melt, which then was dispersed as particles in the impact breccia matrix. The cryptocrystalline melt occurs mainly in sedimentological unit 1 and the lower part of unit 2, which is noteworthy and consistent with their origin near the central peak, the locus of highest temperature and pressure in the impact event. Reworking of part of unit 1 by the interpreted resurge process of unit 2 may have incorporated some melt clasts into the lower part of unit 2. The interpreted melt clasts also are observed to diminish upward in the FC77-1 drill core sequence, which is again consistent with a melt inclusion origin.

CONCLUSIONS

The Flynn Creek impact breccia in drill core FC-77-1, which was drilled on the flank of the central uplift of the Flynn Creek impact structure, consists of 175 m of breccia that lies upon uplifted target strata (drilled to a total depth of 725 m). Within the impact breccia, there are three sedimentological units, each of which is characterized by a distinctive grain size trend.

Sedimentological units 1 (from 175 to 109 m depth) and 3 (from 32 to 0 m depth) have an overall coarsening-upward sequences that we interpret to have been developed by debris and/or rock avalanche processes associated with the flank of the central uplift. Unit 1 may have been mainly a subaqueous deposit, whereas unit 3 is likely to have been mainly subaerial.

Sedimentological unit 2 (from 109 to 32 m depth) is interpreted to have been formed by mass-movement processes off the central uplift's flank and into marine waters within the crater.

The fining-upward sequences and better sorting may be the result of turbiditic flows into standing water within the impact structure.

On the flank of the central uplift, the Flynn Creek impact breccia is composed almost entirely of dolostone clasts and a mainly dolomitic matrix, with minor amounts of chert grains, cryptocrystalline melt clasts, and other particles, including shale clasts and quartz and feldspar grains. No shock-induced features were noted in the quartz and feldspar.

The cryptocrystalline melt clasts are exceedingly fine-grained quartz masses that contain a suite of particles that were derived from the impact event, including carbonate clasts, dolomite crystals, chert fragments, and quartz grains. Even though the melt is very finely crystalline, it appears isotropic when viewed with cross-polarized light. We interpret these melt particles as having formed by melting of minor chert and quartz components in the target strata, and having cooled in such a way that small crystallites (microlites) of quartz formed from the melt. These melt particles, which have not been previously described at Flynn Creek, are confined to sedimentological unit 1 and the lower part of unit 2.

ACKNOWLEDGMENTS

We thank the National Aeronautics and Space Administration, Planetary Geology and Geophysics Program, for supporting the project proposal by J. J. Hagerty and others (NASA PGG NNH14AY73I), of which this publication is a partial result. We also thank the Astrogeology Branch of the U.S. Geological Survey in Flagstaff, Arizona, for organizing the Flynn Creek drill-core collection, hosting our visit to work on these materials, and providing many forms of assistance in sampling. We acknowledge the help of the Geosciences Department at Stony Brook University in allowing access to micro-FTIR and micro-Raman equipment. We thank Rebecca Koch and others for help with core description and photography. The work by J.

Ormö has been partially supported by grants AYA2008-03467⁄ESP, AYA2011-24780/ESP, AYA2012-39362-C02-01, ESP2014-59789-P, and ESP2015-65712-C5-1-R from the Spanish Ministry of Economy and Competitiveness and Fondo Europeo de Desarrollo Regional.

REFERENCES

Azad A. S., Dypvik H., and Kalleson E. 2015. Sedimentation in marine impact craters–Insight from the Ritland impact structure. *Sedimentary Geology* 318:97–112.

Boon J. D. and Albritton C. C. 1936. Meteorite craters and their possible relationship to "cryptovolcanic structures". *Field and Laboratory* 5:1–9.

Conant L. C. and Swanson V. E. 1961. *Chattanooga Shale and related rocks of central Tennessee and nearby areas.* Washington D.C.: U.S. Geological Survey Professional Paper 357. p. 88. 10.

Conrad S. G., Elmore R. T., and Maher S. W. 1954. Stratigraphy of the Chattanooga black shales in the Flynn Creek structure, Jackson County, Tennessee [abstract]. *Geological Society of America Bulletin* 65:1358.

Conrad S. G., Elmore R. T., and Maher S. W. 1957. Stratigraphy of the Chattanooga black shales in the Flynn Creek structure, Jackson County, Tennessee. *Journal of the Tennessee Academy of Science* 32:9–18.

von Dalwigk I. and Ormö J. 2001. Formation of resurge gullies at impacts at sea: The Lockne

crater, Sweden. *Meteoritics & Planetary Science* 36:359–370.

Evenick J. C. and Hatcher R. D. Jr. 2007. Geologic map and cross sections of the Flynn Creek impact structure, Tennessee. GSA Map and Chart Series 95. Boulder, Colorado: Geological Society of America. 1:12,000.

Evenick J. C., Lee P., and Deane B. 2004. Flynn Creek impact structure: New insights from breccias, melt features, shatter cones, and remote sensing (abstract #1131). *35th Lunar and Planetary Science Conference.* CD-ROM.

Folk R. L. 1968. *The petrology of sedimentary rocks.* Austin, Texas: Hemphill's. p. 183.

Gaither T. A., Hagerty J. J., and Bailen M. 2015. The USGS Flynn Creek crater drill core collection: Progress on a web-based portal and online database for the planetary science community (abstract #2089). *46th Lunar and Planetary Science Conference.* CD-ROM.

Gohn G. S., Powars D. S., Bruce T. S., and Self-Trail J. M. 2005. *Physical geology of the impact-modified and impact-generated sediments in the USGS-NASA Langley core.* Hampton, Virginia: U. S. Geological Survey Professional Paper 1688, chapter c:C1–C38.

Hagerty J. J., HcHone J. F., and Gaither T. A. 2013. The Flynn Creek crater drill core collection at the USGS in Flagstaff, Arizona (abstract #2122). *47th Lunar and Planetary Science Conference.* CD-ROM.

Hargrove C. and Rogers A. D. 2013. Thermal infrared and Raman microspectroscopy of moganite-bearing rocks. *American Mineralogist* 98:78–84.

Hungr O. 1990. Momentum transfer and friction in the debris of rock avalanches: Discussion. *Canadian Geotechnical Journal* 27:697.

Hungr O. and Evans S. G. 2004. Entrainment of debris in rock avalanches: An analysis of a long run-out mechanism. *Geological Society of America Bulletin* 116:1240–1252.

Kalleson E., Dypvik H., and Naterstad J. 2008. Post-impact sediments in the Gardnos impact structure, Norway. In *The sedimentary record of meteorite impacts*, edited by Evans K. R., Horton J. W. Jr., King D. T. Jr., and Morrow J. R. Boulder, Colorado: Geological Society of America Special Paper 437. pp. 19–41.

Kieffer S. W. and Simonds C. H. 1980. The Role of Volatiles and Lithology in the Impact Cratering Process. *Review of Geophysics and Space Physics* 18:143–181.

King D. T. Jr., Adrian D. R., Ormö J., Petruny L. W., Hagerty J. J., Gaither T. A., and Jaret S. J. 2015. Flynn Creek impact structure, Tennessee: Its crater-filling breccia in comparison to two other small Paleozoic impact structures and their breccia units. *GSA Abstracts with Programs* 47:A260475.

Lindström M., Ormö J., Sturkell E., and von Dalwigk I. 2005. The Lockne Crater: Revision and reassessment of structure and impact stratigraphy. In *Impact Tectonics*, edited by Koeberl C. and Henkel H. Berlin-Heidelberg: Springer-Verlag. pp. 357–388

Lusk R. G. 1927. A pre-Chattanooga sink hole. *Science* 65:579–580.

Ormö J. and Lindström M. 2000. When a cosmic impact strikes the seabed. *Geological Magazine* 137:67–80.

Ormö J., Hill A. C., and Self-Trail J. M. 2010. A chemostratigraphic method to determine the end of impact-related sedimentation at marine-target impact craters (Chesapeake Bay, Lockne, Tvären). *Meteoritics and Planetary Science* 45: 1206–1224.

Ormö J., Sturkell E., and Lindström M. 2007. Sedimentological analysis of resurge deposits at the Lockne and Tvären craters: Clues to flow dynamics. *Meteoritics & Planetary Science* 42:1929–1943.

Ormö J., Sturkell E., Horton J. W. Jr., Powars D. S., and Edwards L. E. 2009. Comparison of clast frequency and size in the Exmore sediment-clast breccia, Eyreville and Langley cores, Chesapeake Bay impact structure: Clues to the resurge process. In *The ICDP-USGS deep drilling project in the Chesapeake Bay impact structure: Results from the Eyreville coreholes*, edited by Gohn G. S., Koeberl C., Miller K. G., and Reimold W. U. Boulder, Colorado: Geological Society of America Special Paper 458, pp. 617–632.

Osinski G. R., Spray J. G., and Grieve R. A. F. 2008. Impact melting in sedimentary rocks: An assessment. In *The Sedimentary Record of Meteorite Impacts*, edited by Evans K. R., Horton J. W. Jr., King D. T., and Morrow J. R. Boulder, Colorado: Geological Society of America Special Paper 437. pp. 1–18.

Powers M. C. 1953. A new roundness scale for sedimentary particles. *Journal of Sedimentary Petrology* 23:117–119.

Puura V. and Suuroja K. 1992. Ordovician impact crater at Kärdla, Hiiumaa Island, Estonia. *Tectonophysics* 216:143–156.

Roddy D. J. 1966. The Paleozoic crater at Flynn Creek, Tennessee [dissertation]. Pasadena, California: California Institute of Technology. p. 232.

Roddy D. J. 1968. The Flynn Creek crater, Tennessee. In *Shock and metamorphism of natural materials*, edited by French B. M. and Short N. M. Baltimore, Maryland: Mono Book Corporation. pp. 291–322.

Roddy D. J. 1977. Tabular comparisons of the Flynn Creek impact crater, United States, Steinheim impact crater, Germany and Snowball explosion crater, Canada. In *Impact and explosion cratering: Planetary and terrestrial implications (Proceedings of the Symposium on Planetary Cratering Mechanics, Flagstaff, Arizona, September 13–17,*

1976), edited by Roddy D. J., Pepin R. O., and Merrill R. B. New York: Pergamon Press. pp. 125–162.

Roddy D. J. 1979. Structural deformation at the Flynn Creek impact crater, Tennessee: A preliminary report on deep drilling. *Lunar and Planetary Science* 10:2519–2534.

Schieber J. and Over J. D. 2005. Sedimentary fill of the Late Devonian Flynn Creek crater: A hard target marine impact. In *Understanding late devonian and permian-triassic biotic and climatic events: Towards and integrated approach*, edited by Over D. J., Morrow J. R., and Wignall P. B. New York: Elsevier. pp. 51–69.

Shreve R. L. 1968. *The Blackhawk landslide*. Boulder, Colorado: Geological Society of America Special Paper 108. p. 48.

Simon S. 1987. Stratigraphie, Petrographie und Entstehungsbedingungen von Grob-klastika in der autochthonen, Ordovizischen Schichtenfolge Jämtlands (Schweden). *Sveriges Geologiska Undersokning C* 815:1–156.

Sturkell E. F. F. 1998. *Impact-related Ir anomaly in the Middle Ordovician Lockne impact structure.* Jämtland, Sweden: GFF (Geologiska foreningens förhandlingar). 120 (Pt. 4, December):333–336.

Sturkell E., Ormö J., and Lepinette A. 2013. Early modification stage (pre-resurge) sediment

mobilization in the Lockne concentric, marine-target crater, Sweden. *Meteoritics & Planetary Science* 48:321–338.

U. S. Geological Survey, 2017. Mineral Resources On-Line Spatial Data. https://mrdata.usgs.gov/ (Accessed January 2, 2017).

Wilson C. W. and Born K. E. 1936. The Flynn Creek disturbance, Jackson County, Tennessee. *Journal of Geology* 44:815–835.

Witzke B. J. and Anderson R. R. 1996. Sedimentary-clast breccias of the Manson impact structure. In *The Manson impact structure, Iowa: Anatomy of and impact crater,* edited by Koeberl C. and Anderson R. R. Boulder, Colorado: Geological Society of America Special Paper 302. pp. 115–144.

CHAPTER 2

Resurge gullies and the 'inverted sombrero' rim at Flynn Creek impact structure, Tennessee

David R. Adrian and David T. King, Jr.

Department of Geosciences, Auburn University, Auburn, Alabama 36849

Abstract – Flynn Creek impact structure is a small, marine impact structure that is located in north-central Tennessee. The target stratigraphy consists of Lower to Upper Ordovician carbonates, specifically Knox Group through Catheys-Leipers Formation. Like other, similarly sized marine-target impact craters, Flynn Creek's structure-filling deposits consist of gravity-driven avalanche material, washed-back ejecta, and aqueous settling deposits. However, Flynn Creek also possesses previously undescribed erosional resurge gullies and an annular, sloping surface referred to in studies of other marine-target impact structures as the 'rim of an inverted sombrero.' In this paper, we describe these two geomorphic features at Flynn Creek using geographic information system (GIS) technology. We relate these geomorphic features to the marine environment of crater formation, and ultimately compare the Flynn Creek impact structure with other similarly sized marine-target impact structures having similar features.

INTRODUCTION

Located in Jackson County, Tennessee (36° 17' N; 85° 40' W), the Flynn Creek impact structure is a non-circular ("pear-shaped") feature that is at most ~3.8 km in diameter (Fig. 8). This impact structure has a central uplift, a breccia moat, and terraced crater rim, all of which are well defined (Roddy, 1968; 1979; Schieber and Over, 2005; Evenick and Hatcher, 2007). This

impact structure formed when a hypervelocity impact occurred in an epicontinental shelf setting, which was underlain by carbonate bedrock (Roddy, 1966; 1968; 1977; 1979; Schieber and Over, 2005).

In the original U. S. Geological Survey (USGS)-related impact research at Flynn Creek, David Roddy (1966; 1968; 1977; 1979) interpreted the age of impact, based on his observational data, as some time prior to the onset of Chattanooga Shale deposition. Roddy's interpretation thus left open the possibility that this impact structure could actually be much older than Late Devonian, perhaps even Silurian or Ordovician. Subsequent study of the Flynn Creek impact breccia's constituent conodont elemental fauna, which was conducted by Schieber and Over (2005), strongly indicated that the age of impact was in fact early Frasnian (~ 382 m.y.). Our review of all the published evidence pertinent to Flynn Creek's age question suggests to us that Late Devonian is most likely correct (as discussed by Adrian et al., 2017).

The target stratigraphic section was essentially flat-lying Ordovician carbonates including the Lower Ordovician Knox Group through Upper Ordovician Catheys-Leipers Formation (Roddy, 1968; 1979; Evenick and Hatcher, 2007; Gaither et al., 2015). Catheys-Leipers Formation makes up almost all of the Flynn Creek's rim exposures, whereas the central uplift consists primarily of Knox and Stones River Groups and attendant impact-related central uplift-related breccias (Adrian et al., 2017). Figure 8 shows a geological map of the Flynn Creek impact structure and vicinity, which includes these stratigraphic units.

Studies of other small, shallow marine impact structures have shown that immediately following impact, i.e., during the early modification stage of crater development, the crater is filled with gravity-driven avalanche material, washed-back ejecta, and other marine resurge and settling-out deposits (Ormö and Lindström, 2000; von Dalwigk and Ormö, 2001; Suuroja et al.,

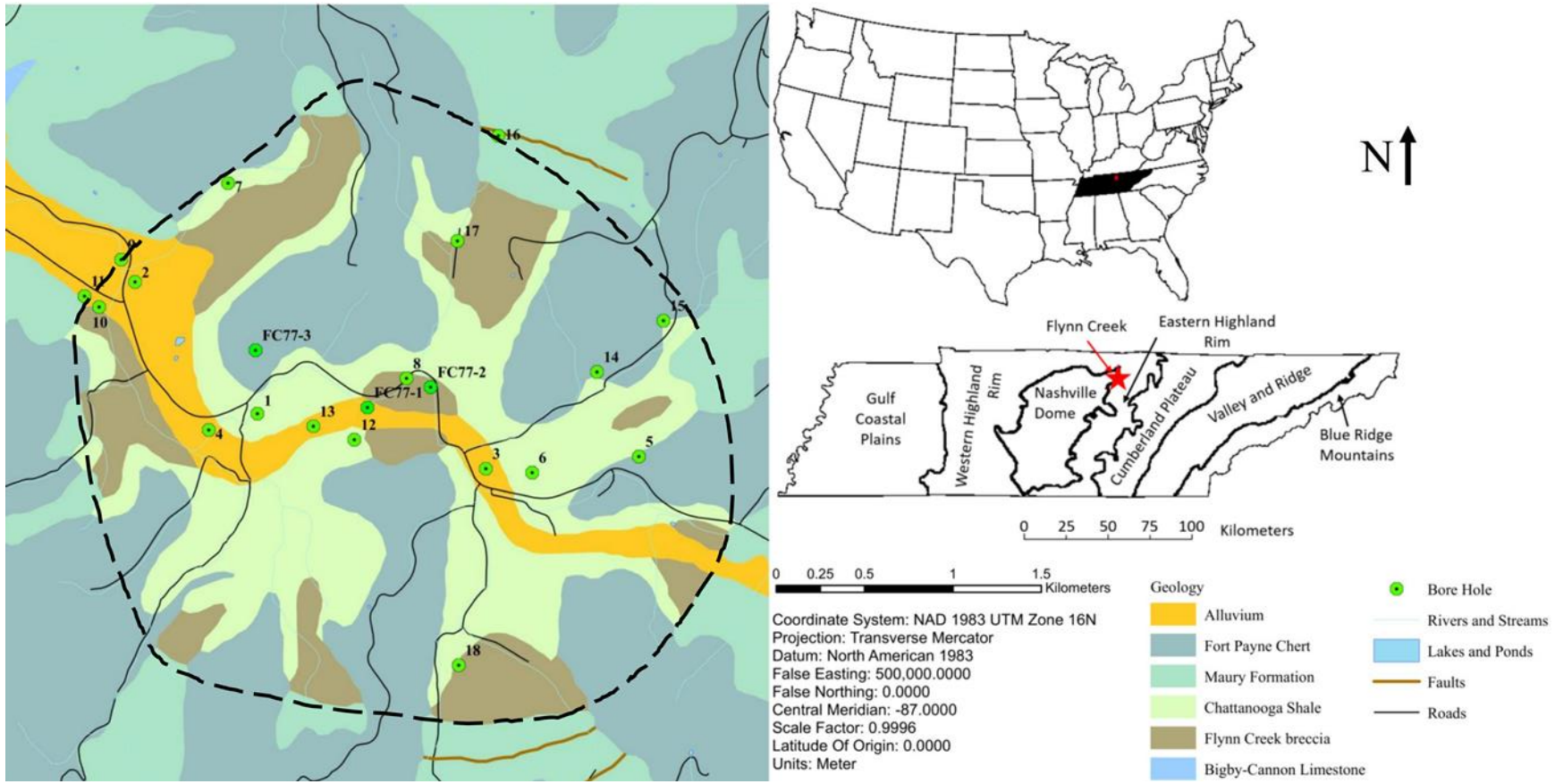
FC77-3
FC77-2
FC77-1
Flynn Creek
Eastern Highland Rim
Gulf Coastal Plains
Western Highland Rim
Nashville Dome
Cumberland Plateau
Valley and Ridge
Blue Ridge Mountains
0 25 50 75 100 Kilometers
0 0.25 0.5 1 1.5 Kilometers
N
Coordinate System: NAD 1983 UTM Zone 16N
Projection: Transverse Mercator
Datum: North American 1983
False Easting: 500,000.0000
False Northing: 0.0000
Central Meridian: -87.0000
Scale Factor: 0.9996
Latitude Of Origin: 0.0000
Units: Meter
Geology
Alluvium
Fort Payne Chert
Maury Formation
Chattanooga Shale
Flynn Creek breccia
Bigby-Cannon Limestone
Bore Hole
Rivers and Streams
Lakes and Ponds
Faults
Roads

Figure 8. Geological map of Flynn Creek impact structure and vicinity. Inset maps show the location of the state of Tennessee in the contiguous United States and the location of the Flynn Creek impact structure on the margin of the Nashville Dome (Eastern Highland Rim area). Colors show the main stratigraphic units, including alluvium and the Fort Payne Formation (post-impact chert), Maury Formation (post-impact shale), Chattanooga Shale (post-impact shale) and Flynn Creek breccia (crater-filling unit). The outcrops of the Catheys-Leipers Formation in the rim area and the Stones River and Knox Groups in the central uplift area are too small to show at the scale of this map. The central uplift is indicated by the central outcrop of Flynn Creek impact breccia (brown), which caps the exposure of the central peak and its flanks. Dashed line shows the asymmetric limit of the impact structure's rim according to Roddy (1968), who conducted extensive field studies in the area. Locations of bore-holes from the USGS-led drilling campaign of 1969-1977, plus three others, are shown with current USGS numbers in the Flynn Creek drill core collection of the USGS Flagstaff (Gaither et al, 2015). Modified from the Flynn Creek map on the U.S. Geological Survey Mineral Resources On-Line Spatial Database (U. S. Geological Survey, 2017a).

2002; Ormö et al., 2007; 2009; 2010; Sturkell et al., 2013; Azad et al., 2015). Flynn Creek impact structure apparently followed this same pattern of early modification stage sedimentation (Adrian et al., 2017; de Marchi et al., 2017).

Beyond their distinctive intra-crater sedimentary characteristics, some marine impact structures may develop resurge gullies (first noted by Ormö and Lindström, 2000; von Dalwigk and Ormö, 2001). Resurge gullies in marine impacts are erosional features made by returning sea water flowing into the crater along localized paths. In addition, marine impact structures may possess a more-or-less concentric, generally inward-dipping surface. This concentric or annular surface, which is both erosional and structural in nature, has been referred to as the "rim" of an "inverted sombrero" (Horton et al., 2005; Gohn et al., 2006). This "rim" is an especially distinctive marine-target crater morphology associated with some marine impact structures, which were formed in layered targets (Horton et al., 2005; Gohn et al., 2006). Similar features (resurge gullies and concentric, gently sloping rims) have been interpreted in marine impact craters on the northern lowland plains of Mars, where there is a noteworthy record of marine impact structures (Ormö et al., 2004; Horton et al., 2006; de Villiers et al., 2010).

Previous work has strongly suggested that Flynn Creek impact structure was subjected to intensive erosion shortly after impact, which we interpret mainly as resurge erosion. For example, Roddy's (1979) study of Flynn Creek ejecta established that the entire Flynn Creek ejecta blanket was removed due to erosion prior to the transgression of the Chattanooga sea. The only known remains of the Flynn Creek ejecta blanket reside in a graben within the southeastern part of the impact structure (Roddy, 1968). We think that most - if not all - of this post-impact erosion likely occurred very early during the crater modification stage, as indicated by the presence of inverse ejecta stratigraphy in the crater-moat filling sequence at Flynn Creek (King et al., 2015; de Marchi et al., 2017).

In a subsequent, post-impact phase, Upper Devonian Chattanooga Shale was deposited within the Flynn Creek impact structure and on the surrounding shelf (Conant and Swanson, 1961; Roddy, 1968; Evenick and Hatcher, 2007). Further, several hundreds of meters of other types of sediments were deposited above the Chattanooga, including the Maury Formation and Fort Payne Chert (see Figure 8; Conant and Swanson, 1961; Roddy, 1968; Evenick and Hatcher, 2007). More recently, erosion in the Flynn Creek area, which occurred in large part because of regional uplift along the Nashville Dome, has generated extensive, dendritic valley networks. These valley networks have cut into the Flynn Creek impact structure and thus dissected its crater rim, walls, floor, and central peak (Roddy, 1979). This valley network provided the extensive erosional exposures used by Roddy (1966; 1968) to map the Flynn Creek impact structure in fine detail, including his precise determination of the elevation control points for his detailed structural contour map of the Flynn Creek impact breccia-Chattanooga Shale contact (Roddy, 1968; 1977; 1990).

In this study, we assess the geomorphologic evidence for resurge gullies and the 'inverted sombrero' rim at Flynn Creek, and relate those features to the marine environment of formation of this hypervelocity impact feature. In the present work, we have digitized the structure contour map of Roddy (1990) and have used geographic information system (GIS) technology to interpret this important structural surface at Flynn Creek.

PREVIOUS WORK

Much of what is known from previous work regarding the Flynn Creek impact structure can be credited to the efforts of David Roddy and other workers at the U. S. Geological Survey during the 1960s and 1970s (Roddy, 1966; 1968; 1977; 1979; 1980). Of particular interest in the present report is the fact that David Roddy very carefully documented the impact structure's outline and the structure-contour elevations regarding the pre-Chattanooga Shale surface, i.e., the Flynn Creek impact breccia-Chattanooga Shale contact. Through intensive field mapping, especially in the rugged stream gullies of the extensive dendritic drainage network that characterizes the Flynn Creek impact area's present topography, Roddy (1966; 1968) carefully measured documented the geology as well as the elevation of the post-crater pre-Chattanooga surface across the whole of the impact structure and vicinity. All this was done at a point in time before any bore-hole data was available. He noted that this structure-contour surface has the same regional structure as that of underlying stratigraphic horizons, except within the impact structure proper. Most of this work was done for his Ph.D. dissertation at Cal Tech (Roddy, 1966), and was distilled later into highly detailed structure-contour maps. These maps were published as figures within two research papers (Roddy, 1968; 1977) and much later on as one large map (Roddy, 1990). In all these reports, Roddy documented small-scale structural highs and lows, structural aspects of the crater rim, irregular valleys eroded into the crater rim and

surrounding area, and other features within the impact structure such as large rock masses (i.e., Roddy's "megabreccia blocks;" see Figures 9 and 10). Roddy's work still stands today as the most detailed field data set about Flynn Creek impact structure.

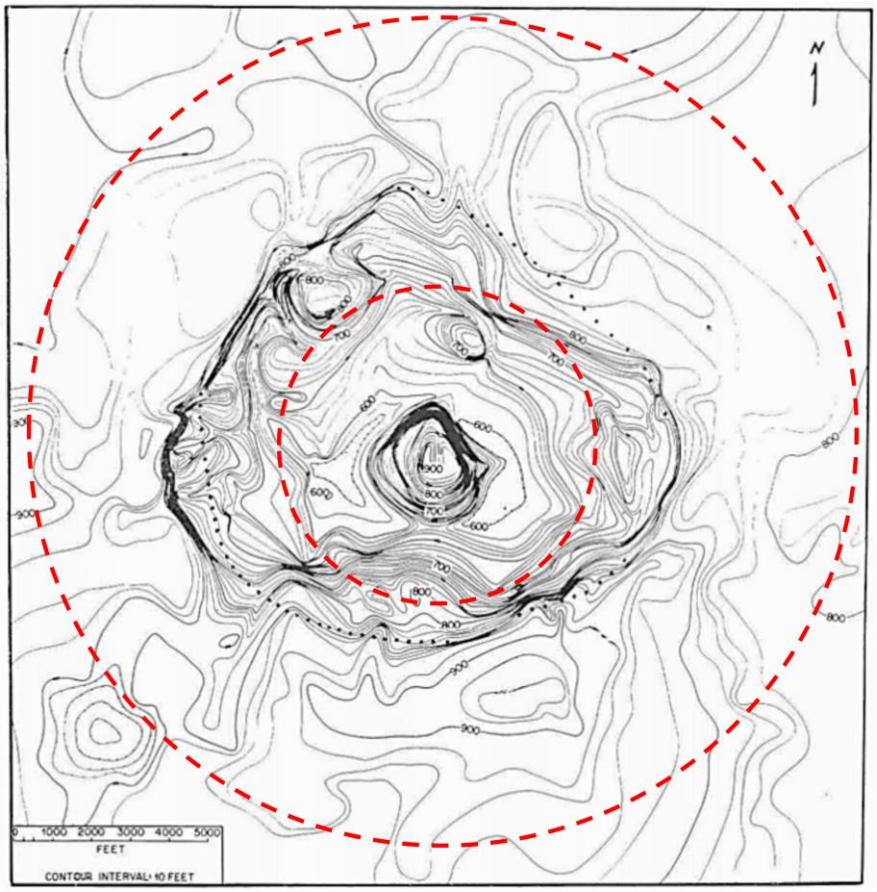

Figure 9. Roddy's (1968) structure contour map of the base of the Chattanooga Shale (i.e., the Chattanooga-Flynn Creek impact breccia contact) within the Flynn Creek impact structure and its vicinity. The dotted line is Roddy's depiction of what he called the "tops of the crater walls," which is the currently accepted, asymmetric outline shape of Flynn Creek impact structure. Of this map, Roddy (1968) wrote that "the contours represent the surface that was present immediately before deposition of the Chattanooga Shale." Regarding this map, Roddy (1966) also notes that the crater walls reveal places "where thick deposits of ejecta were washed into the crater from the rim, or where significant down-faulting and subsidence have occurred to modify the original crater shape." The "large hills" in the northern part of the crater are what Roddy refers to as "megabreccia blocks." Original scale is shown (note that 5000 ft = ~ 1523 m). Structure contour interval is 10 ft, which is ~ 3.05 m. Major structural contour lines are labeled in hundreds of feet. Red dotted line shows our interpretation of the outer limit of the low-sloping concentric area surrounding the deeper inner crater. The low-sloping area is the "rim of the inverted sombrero" and the deeper inner part of the impact structure (i.e., crater bowl) is the "sombrero bowl," as noted in this paper.

Roddy (1966; 1968; 1977; 1990) did not refer to any features at Flynn Creek as 'resurge gullies,' but his structure-contour map clearly showed that there are peripheral valleys (i.e., gullies) and that they deepened toward and connected to the deeper interior part of the impact structure (or crater bowl). Further, his work showed that these gullies cut across a low-sloping surface beyond the dotted outline shown in Figures 9 and 10. This low-sloping area, which concentrically surrounds the impact structure is evident in Roddy's figures but was not discussed in his work. On Figure 9, we have added a dashed line that shows our interpreted outer limit of this low-sloping concentric area. Figures 9 and 10 below show Roddy's depiction of the basal Chattanooga Shale structure-contour map of the Flynn Creek impact structure and vicinity.

Roddy's structure-contour maps and related interpretations came from intensive field work at Flynn Creek, where there are many substantial outcrops and other serendipitous yet small exposures. Following Roddy's extensive field efforts, he also led a drilling and core-collecting campaign in and around the Flynn Creek impact structure, which occurred mainly between 1967 and 1979. This subsurface sampling effort produced more than 3.8 km of nearly continuous drill cores from 18 separate bore holes (Hagerty et al., 2013; Gaither et al., 2015). These bore-hole locations are noted on Figure 8, which also includes three other bore holes that were not part of the USGS-led operation. Roddy (1979; 1980) noted that the bore-hole results agreed with the field mapping studies with regard to the depth and location of the Chattanooga-Flynn Creek impact breccia contact.

He also noted that drill cores from the crater bowl (also called the crater moat) contain thick sequences of re-deposited ejecta. More recent examination of these drill cores reveals a resurge sequence that is overall very similar to marine resurge sequences noted in the crater moats at other marine-target craters (Schieber and Over, 2005; de Marchi et al., 2017).

Figure 10. A "model" of the structure contour map of the Flynn Creek impact structure (taken from Roddy, 1968). This model was constructed from Roddy's (1968) structure contour map, which is shown in Figure 9 above. Roddy's (1968) description of this model says that it shows "the crater shortly before deposition of Chattanooga Shale … The large hills near the outer parts of the crater are underlain by megabreccia blocks derived from the crater walls." The dotted line is the same as in Figure 9. Roddy added that there is "no vertical exaggeration" and that "lighting is from the south." Each "step" or contour interval in this model is 10 ft, which is ~ 3.05 m (same as map in Figure 9).

Schieber and Over (2005) examined four drill cores from Roddy's drilling program and described the crater-filling impact breccias and overlying black shales of the Chattanooga as three distinct units: (1) basal breccia; (2) bedded breccia; and (3) post-impact black shale. Their "basal breccia" and overlying "bedded breccia" correspond to the two-part breccia sequence that

has been noted by King et al. (2015) and de Marchi et al. (2017). Descriptions by de Marchi et al. (2017) showed that the vertical sequence of textures in the (1) basal, non-bedded (or chaotic) breccia and (2) overlying, bedded (or graded) breccia within the crater moat of Flynn Creek impact structure is remarkably similar to dichotomous moat-filling breccia deposits of other marine-target impact structures, such as Lockne and Tvären in Sweden (cf. Ormö et al., 2007; 2010; and Sturkell et al., 2013).

METHODS

We used the 1990 version of Roddy's structure contour map of the Flynn Creek impact breccia-Chattanooga Shale contact, which is a large-format paper map, as the data base for an updated structure contour map. A new digital elevation map of this contact was constructed within ArcGIS (ESRI, 2017). Roddy's 1990 map was chosen for ArcGIS work because it was larger, had more detail, and was much easier to read than the smaller (figure-sized), preliminary structure contour maps and models in Roddy's earlier pertinent work (cf. Roddy, 1968; 1977). As part of our present work in ArcGIS, geospatial data were incorporated in the output. These data were taken from two primary sources: Mineral Resources On-Line Spatial Data (U. S. Geological Survey, 2017a); and The National Map (U. S. Geological Survey, 2017b).

Our GIS-based maps were developed in a series of steps. First, we generated a topographic model for the present topography, which is shown in Figure 11. Second, we generated a new structure contour map using Roddy's (1990) structure contour data (Fig. 12). We then compared the topographic and structure contour data sets to verify the integrity of the structure contour elevations (Fig. 13). Finally, we examined our new structure contour maps for the morphological features that are revealed and delineated the apparent resurge gullies and inward-dipping rim (of the previously mentioned "inverted sombrero" feature).

RESULTS

Figure 11 shows the topographic digital elevation model (DEM) for Flynn Creek and the surrounding area. The drainage pattern shown is strongly dendritic and remarkably shows only minimal influence of the underlying impact structure's annular faults and textural variations. This rendering shows the many stream erosion gullies that afforded Roddy (1966 and subsequent publications) wide access to outcrops in the area, which revealed among other things the elevations of the Flynn Creek impact breccia-Chattanooga Shale contact, which is critical to the present report.

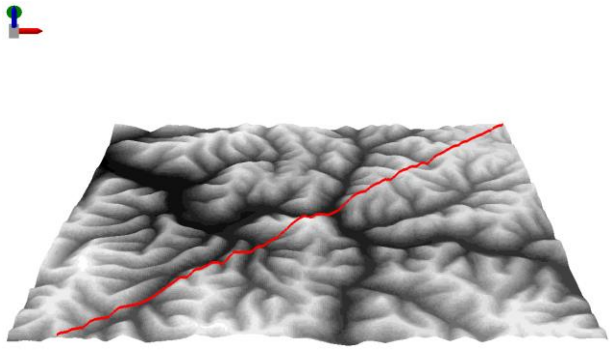

Figure 11. Topographic DEM for the Flynn Creek impact structure and vicinity. This rendering shows a pervasive dendritic drainage pattern that is only minimally influenced by any underlying annular geological structures and their associated, concentrically arranged rock textures. Cross-section (red) line is pertinent to subsequent figures. Area is ~22 km^2.

Figure 12 shows our updated structure contour map, which was constructed for the present report in ArcGIS using the structural contour data set developed from Roddy's (1990) large-scale map. Elevations in Figure 12 are metric, and were converted from Roddy's data given in feet. Elevations are color-coded according to 10-m intervals, as noted on the figure legend. This presentation differs from Roddy's (1990) map only in that he used two different structure-contour intervals (i.e., 10-ft (~ 3.05 m) structure-contour intervals above elevations of

800-feet (~243.84 m) and 50-ft (~15.24 m) structure-contour intervals elsewhere), and we did not change our structure-contour intervals across the area.

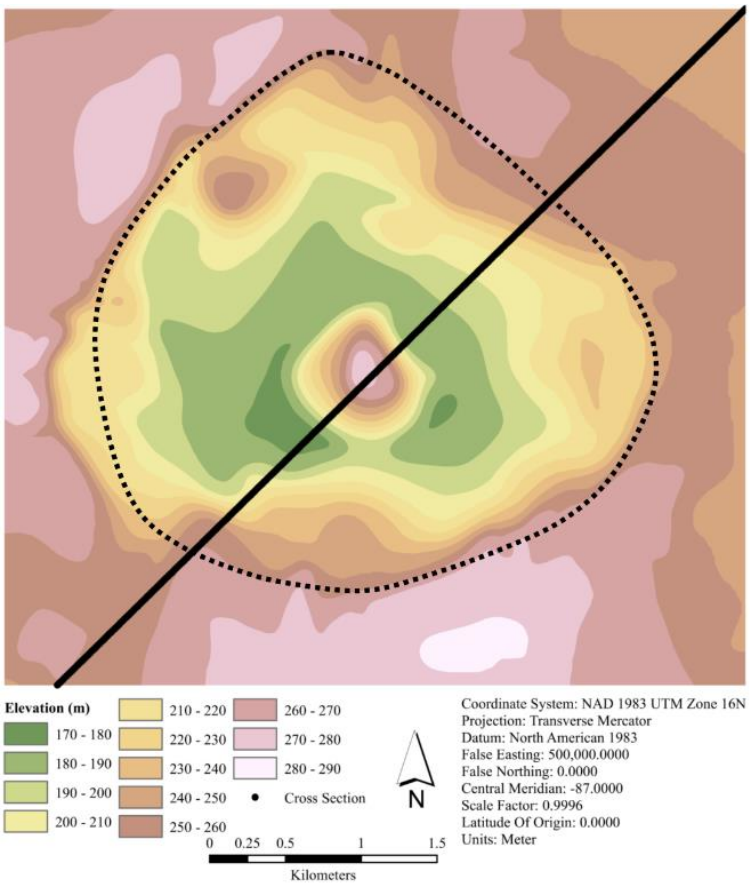

Figure 12. Structure contour map of Flynn Creek impact structure based on elevations of the Flynn Creek impact breccia-Chattanooga Shale contact. Color-coded structure-contour data (elevations for breccia-shale contact) were extracted from the map by Roddy (1990). These data are shown here in 10-m increments (Roddy's data were structure-contour lines of 10 ft). Dotted line is the same "tops of the crater walls" outline (per Roddy, 1968) as in Figures 9 and 10 above. Cross-section (black) line is the same as in Figure 11, and is pertinent to Figure 13. Legend shows elevation color-coding.

Figure 13 shows a cross-sectional view based on our digital elevation models of the topography and the structure-contour map by Roddy (1990). The graph in Figure 13 compares elevations along the cross-section line and shows that the structure contour line's elevations are below the area's topographic elevations. This is important to know because it confirms that Roddy's (1990) observations of structure contour elevations were entirely observable in outcrop.

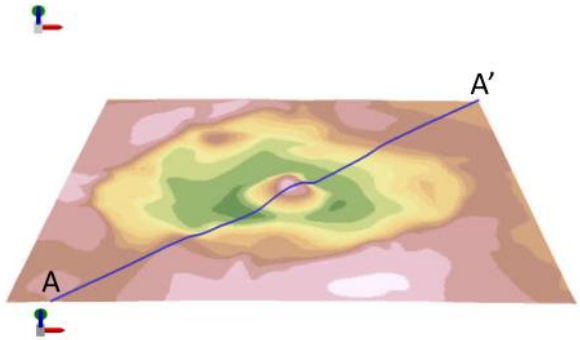
A'
A

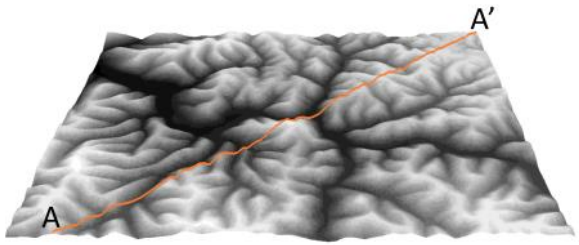
A'
A

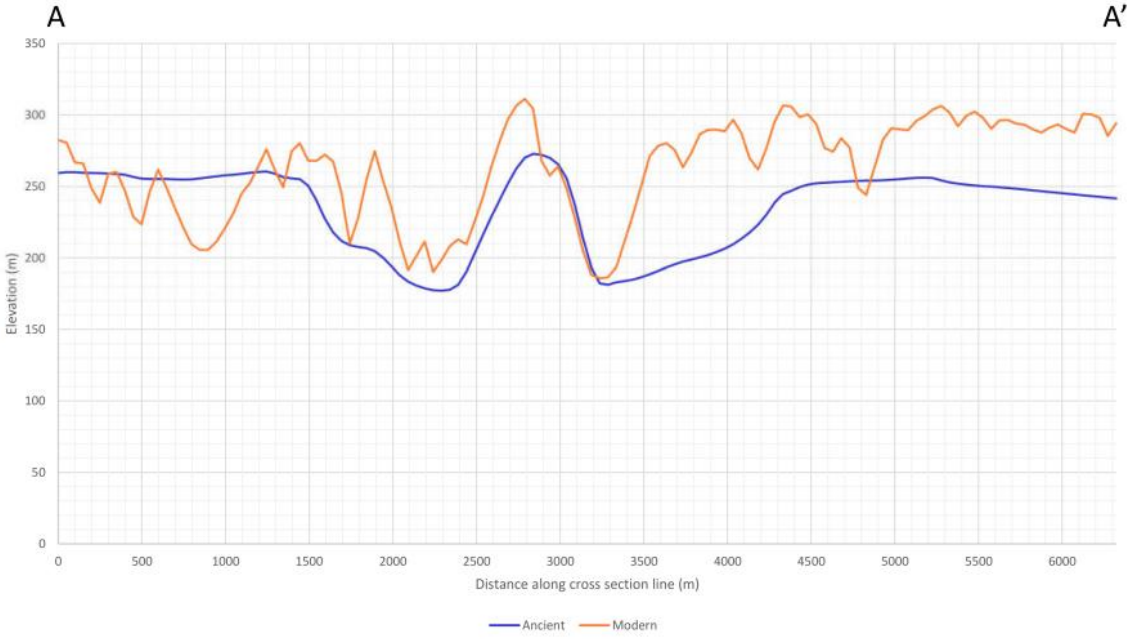
A
A'
350
300
250
200
150
100
50
0
Elevation (m)
0
500
1000
1500
2000
2500
3000
3500
4000
4500
5000
5500
6000
Distance along cross section line (m)
Ancient
Modern

Figure 13. Comparison of the topographic and structural contour elevation models of Figures 11 and 12 along the common cross-section line as shown here and on those figures. The graph at right compares elevations along the cross-section line and shows that the structure contour (smooth, orange line) elevations are below the area's topographic elevations (irregular, blue line). This confirms the fact that Roddy's (1990) observations of structure contour elevations were observable in outcrop and are valid.

Figure 14 shows a merged view of the topographic DEM and the updated structure contour map (Figures 12 and 13, respectively). The topography emerging from the structure contour map level consists of post-impact stratigraphic units and the view below that level shows the color-coded structure-contour map.

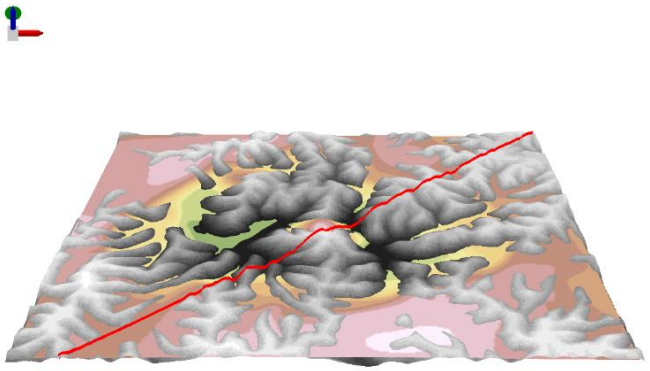

Figure 14. Merged view of the topographic DEM and the color-coded structural contour map, as explained in the text.

Figure 15 is an interpreted cross-section based on structure contour elevations obtained from Roddy (1990) and the elevations of stratigraphic contacts taken from the Flynn Creek map on the U.S. Geological Survey Mineral Resources On-Line Spatial Database (U. S. Geological Survey, 2017a). Additional information was obtained from the drill-core depth records available at the USGS Astrogeology Science Center in Flagstaff for specific drill-core sites. The upper surface in Figure 15 is the modern land surface, whereas the next lower surface is the structure-contour surface in cross-sectional view (i.e., the Flynn Creek impact breccia/Chattanooga Shale contact), which has been moved down so that its details are more clearly seen (cf. Figure 14). In

this cross section, the low-sloping, adjacent surface is the 'inverted sombrero rim' (labeled "sombrero" on Figure 15). This cross section shows that the 'inverted sombrero rim,' which is characteristic of other marine-impact impact structures such as Lockne in Sweden (von Dalwigk and Ormö, 2001) and Chesapeake Bay in Virginia (Gohn et al., 2006), is imperfect.

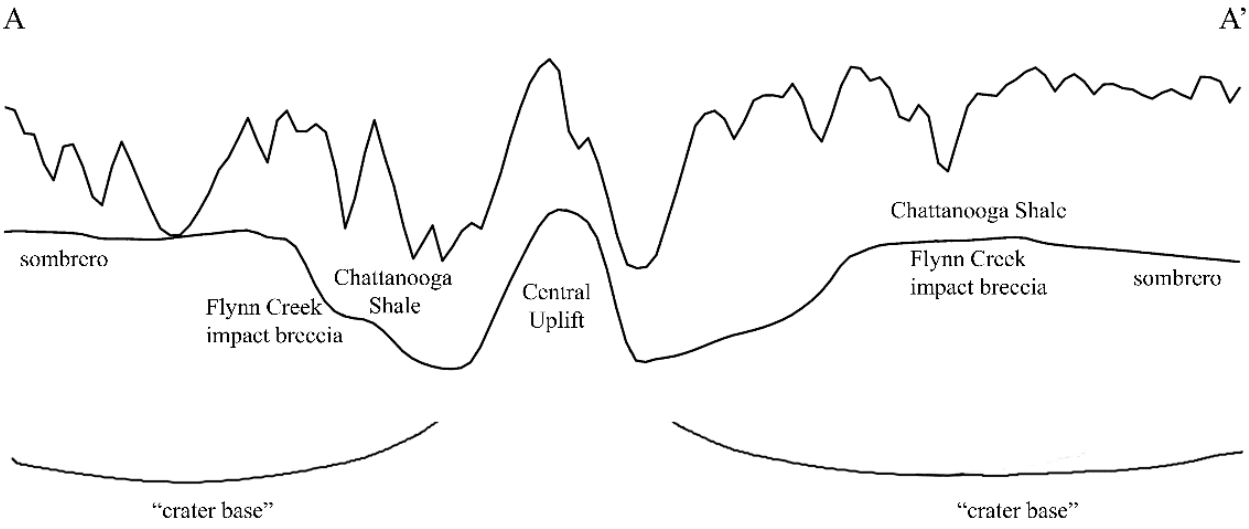

Figure 15. Cross-sectional schematic of Flynn Creek impact structure based on Roddy's (1990) data regarding the Chattanooga-Flynn Creek impact breccia contact and stratigraphic data from the Flynn Creek map on the U.S. Geological Survey Mineral Resources On-Line Spatial Database (U. S. Geological Survey, 2017a). Cross section follows the southwest-northeast cross-section line on previous figures (e.g., Figures 11-14).

Figure 16 shows the interpreted version of the structure contour map in Figure 12, including the main resurge gullies (note that red arrows mark the interpreted *thalweg* of each gully) and the encircling 'inverted sombrero rim.' Gullies cross the 'inverted sombrero rim,' which is larger than the area covered by Roddy's (1990) map, and is thus partially outside the area of Figure 12. The main flow paths (or thalwegs) are shown as superimposed red arrows in Figure 16. They follow the apices of the structure contour lines that define the v-shaped profile of the various aqueous erosional features crossing the impact structure's 'inverted sombrero rim.' To be consistent with previous studies of other marine craters (e.g., von Dalwigk and Ormö,

2001), the ‘inverted sombrero rim’ is regarded the as an adjacent annular area wherein the upper reaches of the resurge gullies are traceable and the structure contour surface is inclined generally toward the crater-moat area.

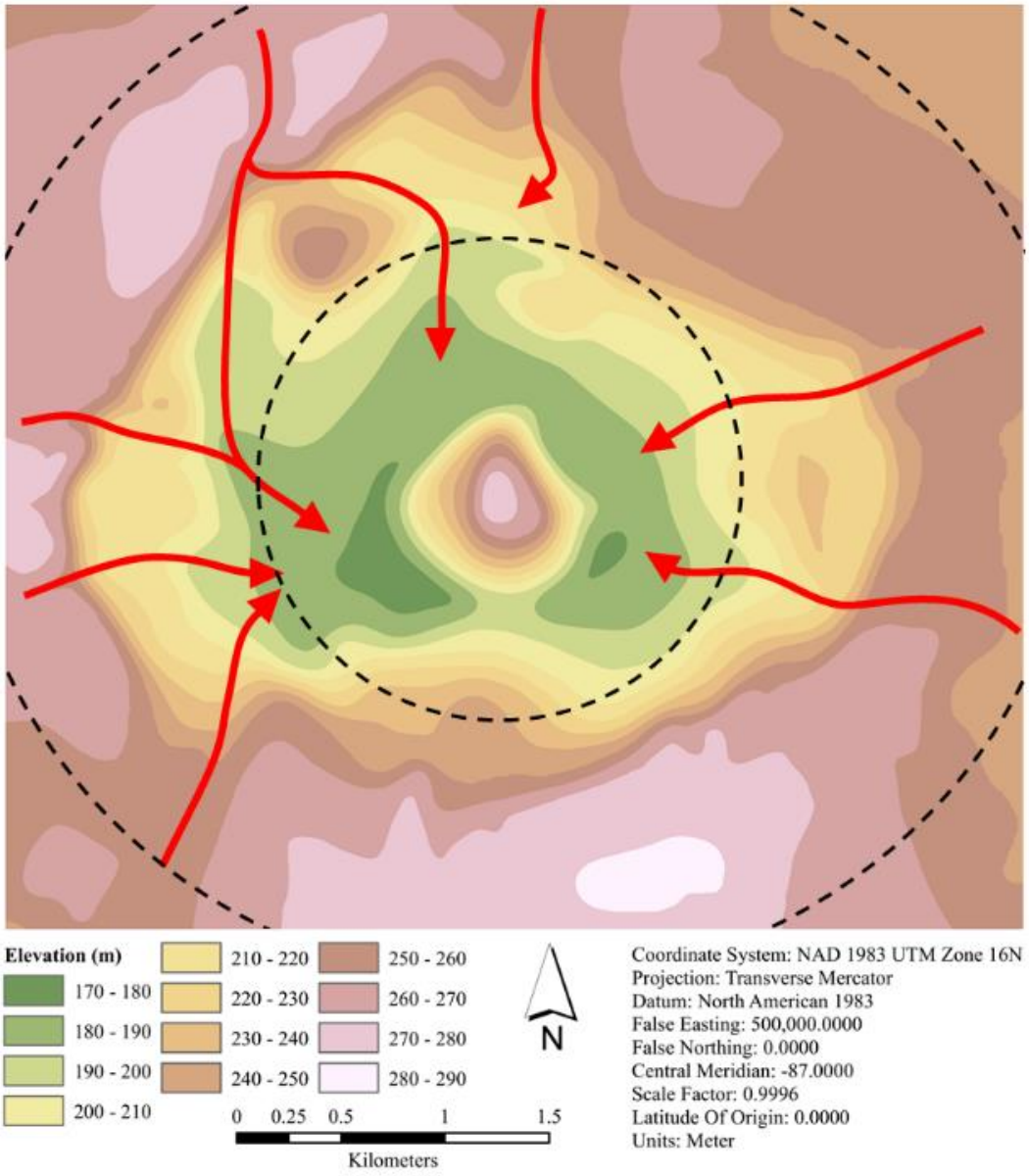

Figure 16. Our DEM model of the structure-contour map of the Flynn Creek impact structure (data taken from Roddy, 1968; see Figure 12 for details). The thalwegs of interpreted resurge gullies, based on the “upstream” v-shape of structure contour lines, are shown as red arrows. The inner, deeper part of the “inverted sombrero” crater shape (i.e., the bowl of the inverted sombrero is outlined by the inner dashed circle and the outer limit of the low-sloping “inverted sombrero rim” is the outer dashed line.

DISCUSSION

Other marine-target impact structures are known to have low-sloping annular areas, which constitute ‘inverted sombrero rims’ (Ormö and Lindström, 2000; von Dalwigk and Ormö, 2001; Suuroja et al., 2002; Ormö et al., 2007; 2009; Sturkell et al., 2013; Azad et al., 2015). Examples include impact structures at Lockne in Sweden (von Dalwigk and Ormö, 2001; Ormö et al., 2007), Kärdla in Estonia (Suuroja et al., 2002); Kamensk in Russia (Ormö and Lindström, 2000), Tvären crater in Sweden (Ormö et al., 2007), and Chesapeake Bay in Virginia (Gohn et al., 2006; Ormö et al., 2009). Figure 17 shows the comparison of essential details of resurge gullies and ‘inverted sombrero rims’ with regard to Lockne and Kärdla, which are the craters most like Flynn Creek. Shown in Figure 17 also is Flynn Creek, with its similar-appearing gullies and ‘inverted sombrero rim.’ For the purposes of comparison, scale is ignored in this figure.

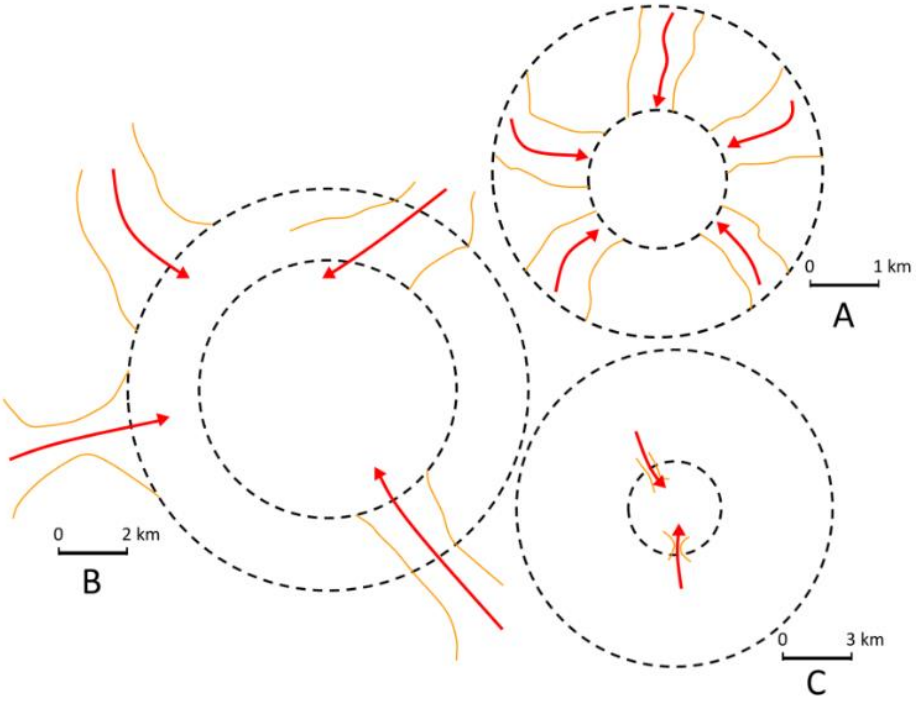

Figure 17. Comparison of 'sombrero rims' (low-sloping, annular surfaces) and resurge gullies at Flynn Creek (A) and two impact structures comparable to Flynn Creek, Lockne (B) and Kärdla (C). Inner crater area and outer limit of the annular rim are shown by nested concentric circles (dashed). Note that scales are different for each crater. Arrows indicate interpreted thalwegs of resurge gullies as inferred from figures within the references cited here (von Dalwigk and Ormö (2001) for Lockne and Ormö and Lindström (2000) for Kärdla).

From these comparable features among well-known and studied marine impact structures, we suggest that the area concentrically surrounding the inner, deeper bowl of these impact structures (i.e., the "rim of the inverted sombrero") and their transecting resurge gullies are all quite similar – if not identical – in nature and origin. The two other examples presented are genetically quite similar, and thus should exhibit comparable effects of marine-water resurge, namely the distinctive gullies and inward-dipping, annular rims. Other marine target impact structures may possess similar tell-tale geomorphic features.

CONCLUSIONS

Flynn Creek impact structure is a marine impact structure that possesses some geomorphic features that are common to many marine impact structures, namely a low-sloping annular rim, with resurge gullies, and a deep interior crater bowl. This is the well-known "inverted sombrero" shape, which was first described at Chesapeake Bay impact structure, and has subsequently been described at Lockne impact structure in Sweden and Kärdla in Estonia, among other places. We know that Flynn Creek impact structure contains a crater-moat filling sequence of resurge breccias, which represent mainly re-deposited proximal ejecta (King et al., 2015; de Marchi et al., 2017), and therefore the return of displaced marine water was an important process in the early modification stage of this impact event. We think that Flynn Creek experienced significant resurge of marine water and thus we see the consequent resurge-related gullies, which have been eroded into the low-sloping annular rim as an expected result of

returning-water flow. Flynn Creek is another example of a marine impact structure that has a geomorphology that is indicative of its marine-impact origin.

ACKNOWLEDGMENTS

We thank the National Aeronautics and Space Administration, Planetary Geology and Geophysics Program, for supporting the project proposal (NASA PGG NNH14AY73I) and we thank the USGS Astrogeology Science Center, Flagstaff, for supporting our work with a subcontract. We also thank the Astrogeology Science Center of the U. S. Geological Survey in Flagstaff, Arizona, for organizing the Flynn Creek drill-core collection, hosting our visits to work on these materials, providing us with data and documents, and providing many other forms of assistance.

REFERENCES

Adrian D. R., King Jr. D. T., Jaret S. J., Ormo J., Petruny L. W., Hagerty J. J., and Gaither T. A. 2017. Sedimentological and petrographic analysis of drill core FC77-1 from the flank of the central uplift, Flynn Creek impact structure, Tennessee. *Meteoritics and Planetary Science* (in press).

Azad A. S., Dypvik H., and Kalleson E. 2015. Sedimentation in marine impact craters–Insight from the Ritland impact structure. *Sedimentary Geology* 318:97–112.

Conant L. C. and Swanson V. E. 1961. *Chattanooga Shale and related rocks of central Tennessee and nearby areas.* Washington D.C.: U.S. Geological Survey Professional Paper 357. p. 88. 10.

von Dalwigk I. and Ormö J. 2001. Formation of resurge gullies at impacts at sea: The Lockne crater, Sweden. *Meteoritics & Planetary Science* 36:359–370.

ESRI (Environmental Systems Research Institute). 2017. ArcGIS. https://www.arcgis.com/home/index.html. (Accessed January 2, 2017).

Evenick J. C. and Hatcher R. D. Jr. 2007. Geologic map and cross sections of the Flynn Creek impact structure, Tennessee. GSA Map and Chart Series 95. Boulder, Colorado: Geological Society of America. 1:12,000.

Gaither T. A., Hagerty J. J., and Bailen M. 2015. The USGS Flynn Creek crater drill core collection: Progress on a web-based portal and online database for the planetary science community (abstract #2089). *46th Lunar and Planetary Science Conference.* CD-ROM.

Gohn G. S., Koeberl C., Miller K. G., Reimold W. U., Cockell C. S., Horton Jr. J. W., Sanford W. E., and Voytek M. A. 2006. Chesapeake Bay impact structure drilled. *Eos, Transactions, American Geophysical Union* 87: 349,355.

Hagerty J. J., HcHone J. F., and Gaither T. A. 2013. The Flynn Creek crater drill core collection at the USGS in Flagstaff, Arizona (abstract #2122). *47th Lunar and Planetary Science Conference.* CD-ROM.

Horton Jr. J. W., Powars D. S., and Gohn G. S. 2005. Studies of the Chesapeake Bay impact structure-Introduction and discussion. In Studies of the Chesapeake Bay impact structure—The USGS-NASA Langley corehole, Hampton, Virginia, and related coreholes and geophysical surveys, edited by Horton Jr. J. W., Powars D. S., and Gohn G. S., U. S. Geological Survey Professional Paper #1688.

Horton Jr. W. J., Ormö J., Powars D. S., and Gohn G. S. 2006. Chesapeake Bay impact structure: Morphology, crater fill, and relevance for impact processes on Mars. *Meteoritics and Planetary Science* 41: 1613–1624.

King Jr. D. T., Adrian D. R., Ormö J., Petruny L. W., Hagerty J. J., Gaither T. A., and Jaret S. J. 2015. Flynn Creek impact structure, Tennessee: Its crater-filling breccia in comparison to other small Paleozoic impact structures and their breccia units. In *6th Planetary Crater Consortium Abstracts*. p. 1502.

de Marchi L., King Jr. D. T., Ormo J., Petruny L. W., Adrian D. R., Hagerty J. J., Gaither T. A., and Jaret S. J. 2017. Marine resurge sequences in drill cores FC67-3 and FC77-3 -- Flynn Creek impact structure, Tennessee USA (abstract #1765). *Lunar and Planetary Science XLVIII (2017).*

Ormö J. and Lindström M. 2000. When a cosmic impact strikes the seabed. *Geological Magazine* 137:67–80.

Ormö J., Fairén A. G., Dohm J. M., Ferris J. C., and Lepinette A. 2004. Marine-target craters on Mars? An assessment study. *Meteoritics and Planetary Science* 39: 333–346.

Ormö J., Sturkell E., and Lindström M. 2007. Sedimentological analysis of resurge deposits at the Lockne and Tvären craters: Clues to flow dynamics. *Meteoritics & Planetary Science* 42:1929–1943.

Ormö J., Sturkell E., Horton J. W. Jr., Powars D. S., and Edwards L. E. 2009. Comparison of clast frequency and size in the Exmore sediment-clast breccia, Eyreville and Langley cores, Chesapeake Bay impact structure: Clues to the resurge process. In *The ICDP-USGS deep drilling project in the Chesapeake Bay impact structure: Results from the Eyreville coreholes*, edited by Gohn G. S., Koeberl C., Miller K. G., and Reimold W. U. Boulder, Colorado: Geological Society of America Special Paper 458, pp. 617–632.

Ormö J., Hill A. C., and Self-Trail J. M. 2010. A chemostratigraphic method to determine the end of impact-related sedimentation at marine-target impact craters (Chesapeake Bay, Lockne, Tvären). *Meteoritics and Planetary Science* 45: 1206–1224.

Roddy D. J. 1966. The Paleozoic crater at Flynn Creek, Tennessee [dissertation]. Pasadena, California: California Institute of Technology. p. 232.

Roddy D. J. 1968. The Flynn Creek crater, Tennessee. In *Shock and metamorphism of natural materials*, edited by French B. M. and Short N. M. Baltimore, Maryland: Mono Book

Corporation. pp. 291–322.

Roddy D. J. 1977. Tabular comparisons of the Flynn Creek impact crater, United States, Steinheim impact crater, Germany and Snowball explosion crater, Canada. In *Impact and explosion cratering: Planetary and terrestrial implications (Proceedings of the Symposium on Planetary Cratering Mechanics, Flagstaff, Arizona, September 13–17, 1976)*, edited by Roddy D. J., Pepin R. O., and Merrill R. B. New York: Pergamon Press. pp. 125–162.

Roddy D. J. 1979. Structural deformation at the Flynn Creek impact crater, Tennessee: A preliminary report on deep drilling. *Lunar and Planetary Science* 10:2519–2534.

Roddy D. J. 1980. Completion of a Deep Drilling Program at the Flynn Creek Impact Crater, Tennessee (abstract #1335). *11th Lunar and Planetary Science Conference*.

Roddy D. J. 1990. Structure Contour Map Drawn on the Base of the Chattanooga Shale Flynn Creek Crater, Gainesboro Quadrangle, Tennessee edited by Hill W. T. Tennessee Division of Geology, Scale 1:12,000.

Schieber J. and Over J. D. 2005. Sedimentary fill of the Late Devonian Flynn Creek crater: A hard target marine impact. In *Understanding late devonian and permian-triassic biotic and climatic events: Towards and integrated approach*, edited by Over D. J., Morrow J. R., and Wignall P. B. New York: Elsevier. pp. 51–69.

Sturkell E., Ormö J., and Lepinette A. 2013. Early modification stage (pre-resurge) sediment mobilization in the Lockne concentric, marine-target crater, Sweden. *Meteoritics & Planetary Science* 48:321–338.

Suuroja K., Suuroja S., All T., and Floden T. 2002. Kärdla (Hiiumaa Island, Estonia) - The buried and well-preserved Ordovician marine impact structure. *Deep-Sea Research Part II: Topical Studies in Oceanography* 49: 1121–1144.

U. S. Geological Survey, 2017a. Mineral Resources On-Line Spatial Data. https://mrdata.usgs.gov/ (Accessed January 2, 2017).

U. S. Geological Survey, 2017b. The National Map. https://nationalmap.gov/ (Accessed January 2, 2017).

de Villiers G., King Jr. D. T., and Marzen L. J. 2010. A study of candidate marine target impact craters in Arabia Terra, Mars. *Meteoritics and Planetary Science* 45: 947–964.

Conclusions

The Flynn Creek impact breccia is situated in the upper 175 m of drill core FC77-1 and is composed almost entirely of dolostone clasts and dolomitic matrix, with only minor amounts of chert grains, cryptocrystalline melt clasts, and other particles, such as shale clasts and quartz and feldspar grains. Within this breccia are three distinct sedimentological units. Unit 1 is a generally coarsening-upward sequence from a depth of 175 to 109 m that was interpreted as developing in a subaqueous debris and/or rock avalanche process during the formation of the central uplift. Unit 2 is an overall fining-upward turbiditic deposit that ranged from a depth of 109 to 32 m and was interpreted to have formed by mass-movement processes off the central uplift's flank and into standing marine waters. Unit 3, from 32 to 0 m depth, was interpreted to have formed under similar conditions as unit 1 except that it mainly formed as a subaerial deposit instead of subaqueous. The melt particles, which have not been previously described at Flynn Creek, are confined to sedimentological unit 1 and the lower part of unit 2. The melt is very finely crystalline, though appears isotropic in cross-polarized light, and was interpreted to have formed by the melting and subsequent cooling of chert and quartz of the target material in such a way that small crystallites (microlites) of quartz formed.

To compliment the sedimentological data attributing a marine impact to some well-known impact craters, geomorphological features associated with many marine impact structures have also been identified, such as resurge gullies and a low-sloping annular rim known as the 'inverted sombrero.' Some impact structures that share these geomorphological features are

Chesapeake Bay in Virgina, USA (Gohn et al., 2006; Ormö et al., 2009), Lockne in Sweden (von Dalwigk and Ormö, 2001; Ormö et al., 2007), and Kärdla in Estonia (Suuroja et al., 2002). In chapter 2, we present evidence for the first time that resurge gullies and the 'inverted sombrero rim' exist at Flynn Creek impact structure as well.

Further research on Flynn Creek impact structure is needed to gain a stronger understanding of the processes associated with its formation in the marine environment and among marine impact craters as a whole. For example, what was the water depth at the time of impact at Flynn Creek and how long was the impact structure eroded prior to deposition of the Chattanooga Shale? While it has been nearly forty years since the completion of David Roddy's drilling campaign, very little data has been recorded, let alone published on the other, nearly 3.8 km of drill core. Other than shatter cones and geomorphological features, the cryptocrystalline melt found as part of this thesis is the only evidence that unequivocally links the formation of this structure to a hypervelocity impact.

Combined References

Adrian D. R., King Jr. D. T., Jaret S. J., Ormo J., Petruny L. W., Hagerty J. J., and Gaither T. A. 2017. Sedimentological and petrographic analysis of drill core FC77-1 from the flank of the central uplift, Flynn Creek impact structure, Tennessee. *Meteoritics and Planetary Science* (in press).

Azad A. S., Dypvik H., and Kalleson E. 2015. Sedimentation in marine impact craters–Insight from the Ritland impact structure. *Sedimentary Geology* 318:97–112.

Boon J. D. and Albritton C. C. 1936. Meteorite craters and their possible relationship to "cryptovolcanic structures". *Field and Laboratory* 5:1–9.

Conant L. C. and Swanson V. E. 1961. *Chattanooga Shale and related rocks of central Tennessee and nearby areas.* Washington D.C.: U.S. Geological Survey Professional Paper 357. p. 88. 10.

Conrad S. G., Elmore R. T., and Maher S. W. 1954. Stratigraphy of the Chattanooga black shales in the Flynn Creek structure, Jackson County, Tennessee [abstract]. *Geological Society of America Bulletin* 65:1358.

Conrad S. G., Elmore R. T., and Maher S. W. 1957. Stratigraphy of the Chattanooga black shales in the Flynn Creek structure, Jackson County, Tennessee. *Journal of the Tennessee Academy of Science* 32:9–18.

von Dalwigk I. and Ormö J. 2001. Formation of resurge gullies at impacts at sea: The Lockne crater, Sweden. *Meteoritics & Planetary Science* 36:359–370.

ESRI (Environmental Systems Research Institute). 2017. ArcGIS. https://www.arcgis.com/home/index.html. (Accessed January 2, 2017).

Evenick J. C. and Hatcher R. D. Jr. 2007. Geologic map and cross sections of the Flynn Creek impact structure, Tennessee. GSA Map and Chart Series 95. Boulder, Colorado: Geological Society of America. 1:12,000.

Evenick J. C., Lee P., and Deane B. 2004. Flynn Creek impact structure: New insights from breccias, melt features, shatter cones, and remote sensing (abstract #1131). *35th Lunar and Planetary Science Conference.* CD-ROM.

Folk R. L. 1968. *The petrology of sedimentary rocks.* Austin, Texas: Hemphill's. p. 183.

Gaither T. A., Hagerty J. J., and Bailen M. 2015. The USGS Flynn Creek crater drill core collection: Progress on a web-based portal and online database for the planetary science community (abstract #2089). *46th Lunar and Planetary Science Conference.* CD-ROM.

Gohn G. S., Koeberl C., Miller K. G., Reimold W. U., Cockell C. S., Horton Jr. J. W., Sanford W. E., and Voytek M. A. 2006. Chesapeake Bay impact structure drilled. *Eos, Transactions, American Geophysical Union* 87: 349,355.

Gohn G. S., Powars D. S., Bruce T. S., and Self-Trail J. M. 2005. *Physical geology of the impact-modified and impact-generated sediments in the USGS-NASA Langley core.* Hampton, Virginia: U. S. Geological Survey Professional Paper 1688, chapter c:C1–C38.

Hagerty J. J., HcHone J. F., and Gaither T. A. 2013. The Flynn Creek crater drill core collection at the USGS in Flagstaff, Arizona (abstract #2122). *47th Lunar and Planetary Science Conference.* CD-ROM.

Hargrove C. and Rogers A. D. 2013. Thermal infrared and Raman microspectroscopy of moganite-bearing rocks. *American Mineralogist* 98:78–84.

Horton Jr. J. W., Powars D. S., and Gohn G. S. 2005. Studies of the Chesapeake Bay impact structure-Introduction and discussion. In Studies of the Chesapeake Bay impact structure—The USGS-NASA Langley corehole, Hampton, Virginia, and related coreholes and geophysical surveys, edited by Horton Jr. J. W., Powars D. S., and Gohn G. S., U. S. Geological Survey Professional Paper #1688.

Horton Jr. W. J., Ormö J., Powars D. S., and Gohn G. S. 2006. Chesapeake Bay impact structure: Morphology, crater fill, and relevance for impact processes on Mars. *Meteoritics and Planetary Science* 41: 1613–1624.

Hungr O. 1990. Momentum transfer and friction in the debris of rock avalanches: Discussion. *Canadian Geotechnical Journal* 27:697.

Hungr O. and Evans S. G. 2004. Entrainment of debris in rock avalanches: An analysis of a long run-out mechanism. *Geological Society of America Bulletin* 116:1240–1252.

Kalleson E., Dypvik H., and Naterstad J. 2008. Post-impact sediments in the Gardnos impact structure, Norway. In *The sedimentary record of meteorite impacts*, edited by Evans K. R., Horton J. W. Jr., King D. T. Jr., and Morrow J. R. Boulder, Colorado: Geological Society of America Special Paper 437. pp. 19–41.

Kieffer S. W., and Simonds C. H. 1980. The Role of Volatiles and Lithology in the Impact Cratering Process. *Review of Geophysics and Space Physics* 18:143–181.

King D. T. Jr., Adrian D. R., Ormö J., Petruny L. W., Hagerty J. J., Gaither T. A., and Jaret S. J. 2015. Flynn Creek impact structure, Tennessee: Its crater-filling breccia in comparison to two other small Paleozoic impact structures and their breccia units. *GSA Abstracts with Programs* 47:A260475.

King Jr. D. T., Adrian D. R., Ormö J., Petruny L. W., Hagerty J. J., Gaither T. A., and Jaret S. J. 2015. Flynn Creek impact structure, Tennessee: Its crater-filling breccia in comparison to other small Paleozoic impact structures and their breccia units. In *6th Planetary Crater Consortium Abstracts*. p. 1502.

Lindström M., Ormö J., Sturkell E., and von Dalwigk I. 2005. The Lockne Crater: Revision and reassessment of structure and impact stratigraphy. In *Impact Tectonics*, edited by Koeberl C. and Henkel H. Berlin-Heidelberg: Springer-Verlag. pp. 357–388

Lusk R. G. 1927. A pre-Chattanooga sink hole. *Science* 65:579–580.

de Marchi L., King Jr. D. T., Ormo J., Petruny L. W., Adrian D. R., Hagerty J. J., Gaither T. A., and Jaret S. J. 2017. Marine resurge sequences in drill cores FC67-3 and FC77-3 -- Flynn Creek impact structure, Tennessee USA (abstract #1765). *Lunar and Planetary Science XLVIII (2017)*.

Ormö J. and Lindström M. 2000. When a cosmic impact strikes the seabed. *Geological Magazine* 137:67–80.

Ormö J., Fairén A. G., Dohm J. M., Ferris J. C., and Lepinette A. 2004. Marine-target craters on Mars? An assessment study. *Meteoritics and Planetary Science* 39: 333–346.

Ormö J., Sturkell E., and Lindström M. 2007. Sedimentological analysis of resurge deposits at the Lockne and Tvären craters: Clues to flow dynamics. *Meteoritics & Planetary Science* 42:1929–1943.

Ormö J., Sturkell E., Horton J. W. Jr., Powars D. S., and Edwards L. E. 2009. Comparison of clast frequency and size in the Exmore sediment-clast breccia, Eyreville and Langley cores, Chesapeake Bay impact structure: Clues to the resurge process. In *The ICDP-USGS deep drilling project in the Chesapeake Bay impact structure: Results from the*

Eyreville coreholes, edited by Gohn G. S., Koeberl C., Miller K. G., and Reimold W. U. Boulder, Colorado: Geological Society of America Special Paper 458, pp. 617–632.

Ormö J., Hill A. C., and Self-Trail J. M. 2010. A chemostratigraphic method to determine the end of impact-related sedimentation at marine-target impact craters (Chesapeake Bay, Lockne, Tvären). *Meteoritics and Planetary Science* 45: 1206–1224.

Osinski G. R., Spray J. G., and Grieve R. A. F. 2008. Impact melting in sedimentary rocks: An assessment. In *The Sedimentary Record of Meteorite Impacts*, edited by Evans K. R., Horton J. W. Jr., King D. T., and Morrow J. R. Boulder, Colorado: Geological Society of America Special Paper 437. pp. 1–18.

Powers M. C. 1953. A new roundness scale for sedimentary particles. *Journal of Sedimentary Petrology* 23:117–119.

Puura V. and Suuroja K. 1992. Ordovician impact crater at Kärdla, Hiiumaa Island, Estonia. *Tectonophysics* 216:143–156.

Roddy D. J. 1966. The Paleozoic crater at Flynn Creek, Tennessee [dissertation]. Pasadena, California: California Institute of Technology. p. 232.

Roddy D. J. 1968. The Flynn Creek crater, Tennessee. In *Shock and metamorphism of natural materials*, edited by French B. M. and Short N. M. Baltimore, Maryland: Mono Book Corporation. pp. 291–322.

Roddy D. J. 1977. Tabular comparisons of the Flynn Creek impact crater, United States, Steinheim impact crater, Germany and Snowball explosion crater, Canada. In *Impact and explosion cratering: Planetary and terrestrial implications (Proceedings of the Symposium on Planetary Cratering Mechanics, Flagstaff, Arizona, September 13–17, 1976)*, edited by Roddy D. J., Pepin R. O., and Merrill R. B. New York: Pergamon Press.

pp. 125–162.

Roddy D. J. 1979. Structural deformation at the Flynn Creek impact crater, Tennessee: A preliminary report on deep drilling. *Lunar and Planetary Science* 10:2519–2534.

Roddy D. J. 1980. Completion of a Deep Drilling Program at the Flynn Creek Impact Crater, Tennessee (abstract #1335). *11th Lunar and Planetary Science Conference*

Roddy D. J. 1990. Structure Contour Map Drawn on the Base of the Chattanooga Shale Flynn Creek Crater, Gainesboro Quadrangle, Tennessee edited by Hill W. T. Tennessee Division of Geology, Scale 1:12,000.

Schieber J. and Over J. D. 2005. Sedimentary fill of the Late Devonian Flynn Creek crater: A hard target marine impact. In *Understanding late devonian and permian-triassic biotic and climatic events: Towards and integrated approach*, edited by Over D. J., Morrow J. R., and Wignall P. B. New York: Elsevier. pp. 51–69.

Shreve R. L. 1968. *The Blackhawk landslide*. Boulder, Colorado: Geological Society of America Special Paper 108. p. 48.

Simon S. 1987. Stratigraphie, Petrographie und Entstehungsbedingungen von Grob-klastika in der autochthonen, Ordovizischen Schichtenfolge Jämtlands (Schweden). *Sveriges Geologiska Undersokning C* 815:1–156.

Sturkell E. F. F. 1998. *Impact-related Ir anomaly in the Middle Ordovician Lockne impact structure.* Jämtland, Sweden: GFF (Geologiska foreningens förhandlingar). 120 (Pt. 4, December):333–336.

Sturkell E., Ormö J., and Lepinette A. 2013. Early modification stage (pre-resurge) sediment mobilization in the Lockne concentric, marine-target crater, Sweden. *Meteoritics & Planetary Science* 48:321–338.

Suuroja K., Suuroja S., All T., and Floden T. 2002. Kärdla (Hiiumaa Island, Estonia) - The buried and well-preserved Ordovician marine impact structure. *Deep-Sea Research Part II: Topical Studies in Oceanography* 49: 1121–1144.

U. S. Geological Survey, 2017a. Mineral Resources On-Line Spatial Data. https://mrdata.usgs.gov/ (Accessed January 2, 2017).

U. S. Geological Survey, 2017b. The National Map. https://nationalmap.gov/ (Accessed January 2, 2017).

de Villiers G., King Jr. D. T., and Marzen L. J. 2010. A study of candidate marine target impact craters in Arabia Terra, Mars. *Meteoritics and Planetary Science* 45: 947–964.

Wilson C. W. and Born K. E. 1936. The Flynn Creek disturbance, Jackson County, Tennessee. *Journal of Geology* 44:815–835.

Witzke B. J. and Anderson R. R. 1996. Sedimentary-clast breccias of the Manson impact structure. In *The Manson impact structure, Iowa: Anatomy of and impact crater*, edited by Koeberl C. and Anderson R. R. Boulder, Colorado: Geological Society of America Special Paper 302. pp. 115–144.

Appendix 1: Thin Section Inventory and Descriptions

A total of 73 standard thin sections were made from samples between 0 to 175 m of well FC77-1, or an average one thin section per 2.4 m of drill core, to fairly represent all three sedimentological units discussed in Chapter 1. Another 17 thin sections, for a total of 90 thin sections, were made to be used for comparison between allocthonous and autochthonous breccias and other material, geochemical analysis in search of a meteoritic trace, and potential future research (Table 1). Thin section reports for each thin section that include more detail and several microphotographs will be archived at the Department of Geosciences at Auburn University.

Sample Label	**Thin Section Labels**	**Description**
77-1-6-A	1-6-A	Brecciated dolomite with brown and green matrix
77-1-10-A	1-10-A	Limestone breccia
77-1-10-B	1-10-B	Limestone breccia
77-1-10-C	1-10-C	Limestone breccia
77-1-10-D	1-10-D	Limestone breccia
77-1-11-A	1-11-A	Breccia
77-1-11-B	1-11-B	Green sand with white clast
77-1-11-C	1-11-C	Breccia dike
77-1-11-D	1-11-D	Fractured white clast
77-1-11-E	1-11-E	Chert
77-1-12-A	1-12-A	Green clay with white clast
77-1-12-B	1-12-B	Greenish sands
77-1-12-C	1-12-C	Fine, greenish sands, chert
77-1-12-E	1-12-E	Sandy
77-1-13-A	1-13-A	Breccia
77-1-15-A	1-15-A	Chert
77-1-15-B	1-15-B	Chert with halo
77-1-16-A	1-16-A	Brecciated dolomite
77-1-17-A	1-17-A	Micro-faults

Sample Label	Thin Section Labels	Description
77-1-18-A	1-18-A	Brecciated dolomite
77-1-19-A	1-19-A	Dark clasts
77-1-20-A	1-20-A	Brecciated dolomite
77-1-22-A	1-22-A	Gray dolomite
77-1-23-A	1-23-A	Breccia
77-1-24-A	1-24-A	Dolomite, very fine grained
77-1-25-A	1-25-A	Dark layer
77-1-25-B	1-25-B	Breccia dike
77-1-28-A	1-28-A	Coarse, white, gray, and brown clasts in dike
77-1-29-A	1-29-A	Dolomite
77-1-29-B	1-29-B	Brecciated cherty interval
77-1-31-A	1-31-A	Brecciated dolomite
77-1-32-A	1-32-A	Dark clasts along matrix change
77-1-34-A	1-34-A	Brecciated dolomite
77-1-35-A	1-35-A	White/green/gray vein
77-1-36-A	1-36-A	Dolomite
77-1-37-A	1-37-A	Dolomite
77-1-38-A	1-38-A	Calcite veinlet in dolomite
77-1-38-B	1-38-B	Yellow stringer
77-1-39-A	1-39-A	Brecciated Dolomite
77-1-40-A	1-40-A	Dolomite, very fine grained
77-1-40-B	1-40-B	Dark matrix filling in cracks of gray vein
77-1-42-A	1-42-A	White rimmed
77-1-43-A	1-43-A	Breccia
77-1-45-A	1-45-A	Brecciated dolomite
77-1-45-B	1-45-B	Melt
77-1-45-C	1-45-C	Melt
77-1-45-D	1-45-D	White melt material
77-1-48-A	1-48-A	Brecciated dolomite
77-1-49-A	1-49-A	White melt vein or melt matrix
77-1-50-A	1-50-A	White flowy carbonate
77-1-50-B	1-50-B	Breccia
77-1-50-C	1-50-C	Mottled matrix
77-1-51-A	1-51-A	Brecciated dolomite
77-1-51-B	1-51-B	Gray chert
77-1-51-C	1-51-C	White vein
77-1-52-A	1-52-A	Breccia
77-1-53-A	1-53-A	Highly mixed breccia

Sample Label	Thin Section Labels	Description
77-1-53-B	1-53-B	Dolomite/chert clasts
77-1-53-C	1-53-C	Breccia with chert clasts
77-1-53-D	1-53-D	Bi-colored chert clast
77-1-53-E	1-53-E	White flowy carbonate; carbonate melt?
77-1-54-A	1-54-A	Highly mixed breccia
77-1-55-A	1-55-A	Highly mixed breccia
77-1-56-A	1-56-A	Breccia with chert clasts
77-1-57-A	1-57-A	Quartz
77-1-57-B	1-57-B	Dolomite/chert clasts
77-1-57-C	1-57-C	Chert
77-1-59-A	1-59-A	Breccia, styolites
77-1-59-B	1-59-B	Possible melt
77-1-59-C	1-59-C	Breccia
77-1-60-A	1-60-A	Breccia, styolites
77-1-60-B	1-60-B	Breccia
77-1-60-C	1-60-C	Breccia with styolites
77-1-61-A	1-61-A	Limestone
77-1-62-A	1-62-A	Styolite/ white dike
79-18-71-A	18-71-A	Representative Knox Group
77-1-78-A	1-78-A	Breccia, styolites
77-1-78-B	1-78-B	Breccia
77-1-83A-A	1-83A-A	Faults
77-1-92-A	1-92-A	White vein, faults
77-1-96-A	1-96-A	Styolites
77-1-113-A	1-113-A	Green matrix with chert nodules
77-1-134-A	1-134-A	Dolomite, microcalc veinlets
77-1-139-A	1-139-A	Breccia
77-1-144-A	1-144-A	White clast/melt
77-1-194-A	1-194-A	Styolite, coarse grains
77-1-209-A	1-209-A	Finer-grained, dark matrix between chert layers
77-1-212-A	1-212-A	Styolite and matrix change
77-1-219-A	1-219-A	Dark and yellow layers
77-1-230-A	1-230-A	Crystalline, does not fizz when acid tested

Table 1. Thin section information made for this study as well as potential future research. 73 thin sections were made from the interval 0 to 175 m or box 60 (ex: 77-1-60-_), which is the main interest of this thesis. Another 17 thin sections were made from drill core outside that interval, including one from well 18, that were mostly used for geochemical analysis as well as comparison.

Appendix 2: Geochemical Analyses

Thirteen drill core cuttings, seven samples from FC77-1 and six reference Knox Group samples from FC79-18, were sent to Bureau Veritas Minerals for two geochemical analyses, Ultra Trace Geochemical aqua regia digestion and Multi-Element Neutron Activation Analysis, in search of a meteoritic trace (Tables 2-5). For Ultra Trace Geochemical aqua regia digestion analysis, all samples were dried at 60°C, individually pulverized to 85% passing 200 (75 microns) mesh using a mild-steel pulverizer. Samples were then digested with a modified Aqua Regia solution of equal parts concentrated HCl, HNO_3 and DI H_2O for one hour in a heating block or hot water bath. Samples were then made up to 15g volume with dilute HCl to then be analyzed.

Maxxam Analytics, a subcontractor for Bureau Veritas Minerals, conducted the Multi-Element Neutron Activation Analysis, a method used for the analysis of elements in samples that have radioactive isotopes with half-lives greater than 1 hour. Each sample was weighed into labelled, plastic vials, a flux monitor was affixed to each vial, and were then inserted into irradiation sites in the core of the reactor where they were then exposed to a neutron flux. Some of the atomic nuclei absorbed neutrons and may have become radioactive. The subsequent decay of these activated nuclei produced a-, b-, and g-radiation, which is characteristic of the decaying elemental isotope. The amounts of the various isotopes, and hence the elements present can be determined by comparison of the spectrum of energies vs. the number of counts at each energy for the samples and standards, which then provides the total amount of element(s) in the sample.

The detection of meteoritic traces in melted or brecciated target rocks is a generally applicable impact-diagnostic method and for small impact structures, which may not show well-developed shock metamorphic effects, such as planar deformation features in rock-forming minerals, the presence of a meteoritic component may be the only factor linking the structure to an impact origin. Though in our case, the geochemical analysis results did not indicate any meteoritic signatures. However, the raw geochemical results have been included here for future researchers and any larger data analysis from this research has be archived at the Department of Geosciences at Auburn University.

Order 1 - FC77-1 Samples															
										Pulp Duplicates		Reference Materials			Prep Wash
		77-1-13-A.1	77-1-53-E.1	77-1-53-E.2	77-1-59-A.1	77-1-59-B.1	77-1-60-A.1	77-1-78-A.1	**Average**	ROCK-VAN	ROCK-VAN	STD DS10	STD OXC129	BLK	ROCK-VAN
Analyte	Unit	Drill Core	Drill Core	Drill Core	Drill Core	Drill Core	Drill Core	Drill Core		Prep Blank	REP	STD	STD	BLK	Prep Blank
Mo	ppm	0.44	0.98	0.39	0.27	0.38	0.32	1.98	**0.68**	1.73	1.65	15.45	1.34	<0.01	1.73
Cu	ppm	3.26	3.78	1.94	1.23	2.01	2.01	1.8	**2.29**	6.2	6.13	162.54	29.22	0.02	6.2
Pb	ppm	0.68	1.64	0.6	0.85	1.55	1.32	0.88	**1.07**	1.49	1.49	154.43	6.8	<0.01	1.49
Zn	ppm	0.8	4.2	1.5	3.9	5.3	12.4	26	**7.7**	31.3	33.2	396.9	44.8	<0.1	31.3
Ag	ppb	37	9	6	9	6	4	5	**11**	21	24	1573	7	<2	21
Ni	ppm	2.9	4.4	2	1.4	3.1	2.8	7	**3.4**	1.8	1.8	78.1	84.5	<0.1	1.8
Co	ppm	1.2	1.4	0.5	0.6	1.2	1.1	3.2	**1.3**	3.9	3.8	13.4	21.8	<0.1	3.9
Mn	ppm	63	78	77	44	51	51	59	**60**	441	435	866	431	<1	441
Fe	%	0.11	0.33	0.2	0.16	0.23	0.24	0.47	**0.25**	1.81	1.81	2.76	3.06	<0.01	1.81
As	ppm	1.5	3.2	1.1	0.7	1.5	1.1	4.5	**1.9**	1.3	1.3	43	0.6	0.1	1.3
U	ppm	0.7	1.2	1.1	0.2	0.2	0.3	0.3	**0.6**	0.4	0.4	2.7	0.7	<0.1	0.4
Au	ppb	0.7	<0.2	0.2	<0.2	0.4	<0.2	<0.2	**0.4**	0.8	0.9	75.1	197.4	<0.2	0.8
Th	ppm	0.2	0.8	0.5	0.3	0.8	0.6	0.8	**0.6**	2.3	2.3	7.8	2	<0.1	2.3
Sr	ppm	110.1	113.5	134	164.6	190.5	215.7	111	**148.5**	31.3	29.7	66.8	191.5	<0.5	31.3
Cd	ppm	0.01	0.01	<0.01	0.05	0.03	0.01	0.13	**0.04**	0.04	0.03	2.36	0.03	<0.01	0.04
Sb	ppm	0.03	0.07	0.02	<0.02	<0.02	<0.02	0.04	**0.04**	0.06	0.04	8.74	0.03	<0.02	0.06
Bi	ppm	0.14	<0.02	<0.02	<0.02	<0.02	<0.02	0.03	**0.09**	<0.02	<0.02	11.69	<0.02	<0.02	<0.02
V	ppm	7	8	8	2	4	3	5	**5**	24	24	45	53	<2	24
Ca	%	17.67	15.46	18.55	27.72	26.75	27.78	19.28	**21.89**	0.64	0.62	1.05	0.65	<0.01	0.64
P	%	0.002	0.005	0.003	0.003	0.004	0.005	0.016	**0.005**	0.038	0.039	0.069	0.097	<0.001	0.038
La	ppm	1.6	2.1	2.6	1.6	2.3	2.2	1.8	**2.0**	5.7	5.7	18.2	13.7	<0.5	5.7
Cr	ppm	2.4	5.2	2.8	1.7	2.9	2.7	3.5	**3.0**	3.9	4	57.5	54.5	<0.5	3.9
Mg	%	10	7.91	9.64	2.67	2.54	2.23	4.32	**5.62**	0.38	0.37	0.77	1.53	<0.01	0.38
Ba	ppm	2.5	12.7	9.1	451.7	21	19.3	5.1	**74.5**	73.1	72.7	327.5	49.1	<0.5	73.1
Ti	%	<0.001	0.001	<0.001	<0.001	<0.001	<0.001	<0.001	**0.001**	0.09	0.09	0.085	0.417	<0.001	0.09
B	ppm	4	5	3	5	8	6	12	**6**	2	<1	7	2	<1	2
Al	%	0.09	0.12	0.09	0.09	0.18	0.19	0.21	**0.14**	0.92	0.92	1.05	1.51	<0.01	0.92
Na	%	0.025	0.021	0.018	0.013	0.016	0.02	0.036	**0.021**	0.102	0.103	0.07	0.584	<0.001	0.102
K	%	0.05	0.08	0.05	0.05	0.11	0.11	0.15	**0.09**	0.1	0.1	0.33	0.36	<0.01	0.1
W	ppm	<0.1	<0.1	<0.1	<0.1	<0.1	<0.1	<0.1	**<0.1**	0.1	0.1	3	<0.1	<0.1	0.1
Sc	ppm	0.4	0.6	0.5	0.4	0.7	0.9	1	**0.6**	2.6	2.6	2.8	0.7	<0.1	2.6
Tl	ppm	<0.02	0.05	<0.02	<0.02	0.04	0.03	0.04	**0.04**	<0.02	<0.02	4.88	0.03	<0.02	<0.02
S	%	0.03	0.17	0.09	0.1	0.17	0.16	0.35	**0.15**	<0.02	<0.02	0.27	<0.02	<0.02	<0.02
Hg	ppb	<5	5	7	<5	<5	7	<5	**6**	<5	<5	246	<5	<5	<5
Se	ppm	<0.1	<0.1	<0.1	<0.1	<0.1	<0.1	<0.1	**<0.1**	<0.1	<0.1	2.4	<0.1	<0.1	<0.1
Te	ppm	<0.02	<0.02	0.03	<0.02	0.04	0.03	<0.02	**0.03**	<0.02	<0.02	4.67	<0.02	<0.02	<0.02
Ga	ppm	0.1	0.4	0.2	0.2	0.3	0.5	0.3	**0.3**	4	3.9	4.5	5.4	<0.1	4
Pr	ppm	0.37	0.45	0.57	0.44	0.63	0.68	0.65	**0.54**	1.37	1.4	4	2.74	<0.02	1.37
Nd	ppm	1.17	1.93	2.16	1.65	2.3	2.21	2.57	**2.00**	6.03	5.88	15.08	10.14	<0.02	6.03
Sm	ppm	0.13	0.19	0.52	0.34	0.51	0.38	0.49	**0.37**	1.14	1.25	2.73	1.61	<0.02	1.14
Eu	ppm	0.06	0.09	0.08	0.07	0.12	0.1	0.11	**0.09**	0.27	0.22	0.52	0.48	<0.02	0.27
Gd	ppm	0.16	0.19	0.3	0.24	0.41	0.33	0.39	**0.29**	1.37	1.39	2.11	1.19	<0.02	1.37
Tb	ppm	0.03	0.04	0.05	0.05	0.06	0.07	0.08	**0.05**	0.22	0.21	0.28	0.2	<0.02	0.22
Dy	ppm	0.16	0.18	0.25	0.26	0.29	0.3	0.44	**0.27**	1.44	1.41	1.53	1.04	<0.02	1.44
Ho	ppm	0.03	0.04	0.05	0.04	0.06	0.07	0.09	**0.05**	0.32	0.33	0.32	0.19	<0.02	0.32
Er	ppm	0.08	0.15	0.17	0.17	0.13	0.19	0.27	**0.17**	0.83	0.82	0.91	0.48	<0.02	0.83
Tm	ppm	<0.02	<0.02	0.02	<0.02	<0.02	0.02	0.03	**0.02**	0.15	0.14	0.11	0.07	<0.02	0.15
Yb	ppm	0.05	0.1	0.08	0.1	0.11	0.19	0.2	**0.12**	0.94	1.03	0.68	0.42	<0.02	0.94
Lu	ppm	<0.02	<0.02	<0.02	0.02	<0.02	0.03	0.02	**0.02**	0.11	0.13	0.13	0.06	<0.02	0.11

Table 2. Raw results from Ultra Trace Geochemical aqua regia digestion analysis of seven samples from various depths of well FC77-1 provided by Bureau Veritas Minerals. Samples were chosen from their lithologies and associated likelihood of containing a meteoritic trace.

Order 2 - FC79-18 Samples (Representative Knox)														
									Pulp Duplicates		Reference Materials			Prep Wash
		79-18-71-A.1	79-18-73-A.1	79-18-74-A.1	79-18-75-A.1	79-18-76-A.1	79-18-77-A.1	**Average**	79-18-77-A.1	79-18-77-A.1	STD DS10	STD OXC129	BLK	ROCK-VAN
Analyte	Unit	Drill Core	Drill Core	Drill Core	Drill Core	Drill Core	Drill Core		Drill Core	REP	STD	STD	BLK	Prep Blank
Mo	ppm	0.3	0.17	0.42	0.15	0.33	0.24	**0.27**	0.24	0.24	14.88	1.23	<0.01	0.96
Cu	ppm	1.42	1.82	0.54	1.51	4.5	3.18	**2.16**	3.18	2.95	150.68	26.47	<0.01	7.2
Pb	ppm	1.9	2.15	0.76	1.83	3.45	2.98	**2.18**	2.98	2.93	148.27	6.15	<0.01	2.01
Zn	ppm	3.6	3.3	2.1	3.9	9	6.3	**4.7**	6.3	6.1	369	39.7	<0.1	30.6
Ag	ppb	4	2	<2	3	4	7	**4**	7	4	1919	12	<2	26
Ni	ppm	2.9	3.4	1.2	2.8	8.5	6	**4.1**	6	6.4	72.5	76.2	<0.1	1.1
Co	ppm	1.1	1.3	0.5	1.1	3.9	2.9	**1.8**	2.9	2.9	12.9	19.5	<0.1	3.7
Mn	ppm	127	206	219	208	150	132	**174**	132	131	878	409	<1	445
Fe	%	0.31	0.32	0.33	0.36	0.65	0.68	**0.44**	0.68	0.67	2.79	3.06	<0.01	1.83
As	ppm	1.8	1.2	1.5	1.1	2	4.6	**2.0**	4.6	4.3	46.4	0.6	<0.1	1.5
U	ppm	0.4	0.3	0.2	0.3	0.3	0.5	**0.3**	0.5	0.5	2.7	0.7	<0.1	0.5
Au	ppb	0.5	1.2	0.4	<0.2	1.5	0.3	**0.8**	0.3	0.2	73.2	191.1	<0.2	1
Th	ppm	0.5	0.5	0.1	0.5	1.2	1	**0.6**	1	1	7.3	1.8	<0.1	2.4
Sr	ppm	141.9	79.2	81.9	122.3	114.6	141.4	**113.6**	141.4	141	66.4	187	<0.5	30.2
Cd	ppm	0.03	0.02	0.02	0.01	<0.01	<0.01	**0.02**	<0.01	0.01	2.81	0.05	<0.01	0.04
Sb	ppm	0.05	0.06	0.04	0.02	0.03	0.16	**0.06**	0.16	0.14	8.81	0.03	<0.02	0.05
Bi	ppm	<0.02	<0.02	<0.02	<0.02	0.05	0.03	**0.04**	0.03	0.03	12.52	<0.02	<0.02	0.04
V	ppm	4	3	<2	2	5	4	**4**	4	4	43	50	<2	22
Ca	%	18.6	18.33	19.88	20.69	14.97	17.94	**18.40**	17.94	17.57	1.06	0.66	<0.01	0.61
P	%	0.003	0.003	0.002	0.004	0.01	0.01	**0.005**	0.01	0.01	0.072	0.098	<0.001	0.04
La	ppm	1.4	1.4	0.9	2.2	3.2	2.6	**2.0**	2.6	2.6	18	12.2	<0.5	5.9
Cr	ppm	4.4	4.3	1.7	3	5	4.2	**3.8**	4.2	4.1	53.8	48.4	<0.5	4
Mg	%	9.42	11.25	11.82	10.49	8.01	9.53	**10.09**	9.53	9.35	0.78	1.52	<0.01	0.39
Ba	ppm	8.3	5.1	3	48.9	15.9	15	**16.0**	15	14.8	353.6	49.7	<0.5	82
Ti	%	0.002	<0.001	<0.001	<0.001	<0.001	<0.001	**0.002**	<0.001	<0.001	0.081	0.385	<0.001	0.088
B	ppm	28	24	3	16	17	30	**20**	30	29	7	2	<1	2
Al	%	0.17	0.18	0.05	0.15	0.33	0.32	**0.20**	0.32	0.32	1.08	1.65	<0.01	1.08
Na	%	0.031	0.026	0.027	0.027	0.043	0.039	**0.032**	0.039	0.039	0.074	0.623	<0.001	0.181
K	%	0.1	0.11	0.02	0.08	0.16	0.16	**0.11**	0.16	0.16	0.34	0.41	<0.01	0.16
W	ppm	<0.1	<0.1	<0.1	<0.1	<0.1	<0.1	**<0.1**	<0.1	<0.1	3.2	<0.1	<0.1	0.1
Sc	ppm	0.8	1	0.3	0.9	1.9	1.6	**1.1**	1.6	1.6	3	0.8	<0.1	2.8
Tl	ppm	<0.02	0.02	0.03	0.02	0.03	0.06	**0.03**	0.06	0.06	5.16	0.03	<0.02	<0.02
S	%	0.12	0.11	0.04	0.18	0.42	0.52	**0.23**	0.52	0.52	0.27	<0.02	<0.02	<0.02
Hg	ppb	<5	<5	<5	<5	8	<5	**8**	<5	<5	277	<5	<5	<5
Se	ppm	<0.1	0.1	<0.1	<0.1	<0.1	<0.1	**0.1**	<0.1	<0.1	2.5	<0.1	<0.1	<0.1
Te	ppm	0.02	0.03	0.02	0.04	0.02	0.03	**0.03**	0.03	0.03	4.96	<0.02	<0.02	<0.02
Ga	ppm	0.6	0.6	0.1	0.5	1.1	1.1	**0.7**	1.1	1	4.6	5.5	<0.1	4.2
Pr	ppm	0.44	0.46	0.26	0.61	1.11	0.88	**0.63**	0.88	0.88	3.95	2.43	<0.02	1.48
Nd	ppm	1.72	1.72	1.16	2.5	4.85	3.72	**2.61**	3.72	3.8	14.54	8.84	<0.02	6.11
Sm	ppm	0.34	0.35	0.19	0.51	1.04	0.76	**0.53**	0.76	0.81	2.55	1.53	<0.02	1.24
Eu	ppm	0.08	0.08	0.04	0.1	0.22	0.16	**0.11**	0.16	0.18	0.47	0.47	<0.02	0.28
Gd	ppm	0.3	0.28	0.2	0.54	1.07	0.66	**0.51**	0.66	0.71	2.05	1.26	<0.02	1.35
Tb	ppm	0.03	0.03	<0.02	0.06	0.15	0.11	**0.08**	0.11	0.11	0.29	0.18	<0.02	0.24
Dy	ppm	0.18	0.23	0.17	0.42	0.95	0.65	**0.43**	0.65	0.69	1.56	1.02	<0.02	1.53
Ho	ppm	0.04	0.05	0.03	0.08	0.18	0.12	**0.08**	0.12	0.11	0.3	0.17	<0.02	0.3
Er	ppm	0.13	0.13	0.06	0.23	0.42	0.32	**0.22**	0.32	0.32	0.8	0.38	<0.02	0.92
Tm	ppm	<0.02	<0.02	<0.02	0.03	0.06	0.04	**0.04**	0.04	0.04	0.12	0.06	<0.02	0.13
Yb	ppm	0.11	0.11	0.05	0.2	0.35	0.32	**0.19**	0.32	0.29	0.81	0.38	<0.02	0.86
Lu	ppm	<0.02	<0.02	<0.02	0.02	0.05	0.03	**0.03**	0.03	0.04	0.11	0.05	<0.02	0.13

Table 3. Raw results from Ultra Trace Geochemical aqua regia digestion analysis of six samples from various depths of well FC79-18 provided by Bureau Veritas Minerals. These samples were chosen to act as our "control" group, or our non-impact related Knox Group rocks to determine if there was any meteoritic trace left, at least in these samples.

Order 1 - FC77-1 Samples - INAA											
	UNITS	77-1-13-A.1	77-1-53-E.1	77-1-53-E.2	77-1-59-A.1	77-1-59-B.1	77-1-60-A.1	77-1-78-A.1	**Average**	Reportable Detection Limit	Quality Control Batch
Bromine	ppm	1.3	0.9	<0.5	0.6	<0.5	1.5	0.8	**1**	0.5	4557306
Antimony (Sb)	ppm	<0.1	0.1	<0.1	<0.1	<0.1	<0.1	<0.1	**0**	0.1	4557306
Arsenic (As)	ppm	1.1	3.6	1.2	0.8	0.9	0.9	4.4	**2**	0.5	4557306
Barium (Ba)	ppm	<50	56	<50	710	<50	<50	<50	**383**	50	4557306
Calcium (Ca)	ppm	170000	150000	170000	280000	240000	280000	170000	**208571**	10000	4557306
Cerium (Ce)	ppm	3	4	5	5	6	7	9	**6**	3	4557306
Cesium (Cs)	ppm	<1	<1	<1	<1	<1	<1	<1	**<1**	1	4557306
Chromium (Cr)	ppm	<5	9	<5	5	8	8	12	**8**	5	4557306
Cobalt (Co)	ppm	1	1	<1	1	2	1	4	**2**	1	4557306
Europium (Eu)	ppm	<0.2	<0.2	<0.2	<0.2	<0.2	<0.2	<0.2	**<0.2**	0.2	4557306
Gold (Au)	ppm	<0.002	<0.002	<0.002	<0.002	<0.002	<0.002	<0.002	**<0.002**	0.002	4557306
Hafnium (Hf)	ppm	<1	<1	<1	<1	<1	<1	<1	**<1**	1	4557306
Iridium (Ir)	ppm	<0.005	<0.005	<0.005	<0.005	<0.005	<0.005	<0.005	**<0.005**	0.005	4557306
Iron (Fe)	ppm	1500	4100	2600	2300	3200	3200	6900	**3400**	100	4557306
Lanthanum (La)	ppm	1.6	2	2.4	2.4	3	3.4	4.4	**3**	0.5	4557306
Lutetium (Lu)	ppm	<0.05	<0.05	<0.05	<0.05	<0.05	<0.05	<0.05	**<0.05**	0.05	4557306
Mercury (Hg)	ppm	<1	<1	<1	<1	<1	<1	<1	**<1**	1	4557306
Molybdenum (Mo)	ppm	<1	<1	<1	<1	<1	<1	1	**1**	1	4557306
Neodymium (Nd)	ppm	<5	<5	<5	<5	<5	<5	<5	**<5**	5	4557306
Nickel (Ni)	ppm	<100	<100	<100	<100	<100	<100	<100	**<100**	100	4557306
Rubidium (Rb)	ppm	<15	<15	<15	<15	17	<15	23	**20**	15	4557306
Samarium (Sm)	ppm	0.2	0.3	0.4	0.4	0.5	0.6	0.7	**0**	0.1	4557306
Scandium (Sc)	ppm	0.4	0.9	0.6	0.7	1.3	1.4	2	**1**	0.1	4557306
Selenium (Se)	ppm	<3	<3	<3	<3	<3	<3	<3	**<3**	3	4557306
Silver (Ag)	ppm	<5	<5	<5	<5	<5	<5	<5	**<5**	5	4557306
Sodium (Na)	ppm	270	290	210	200	230	270	510	**283**	100	4557306
Strontium (Sr)	ppm	<500	<500	<500	<500	<500	<500	<500	**<500**	500	4557306
Tantalum (Ta)	ppm	1.1	0.7	1.6	0.5	<0.5	0.5	<0.5	**1**	0.5	4557306
Terbium (Tb)	ppm	<0.5	<0.5	<0.5	<0.5	<0.5	<0.5	<0.5	**<0.5**	0.5	4557306
Thorium (Th)	ppm	0.3	0.8	0.5	0.6	1	0.9	1.4	**1**	0.2	4557306
Tin (Sn)	ppm	<100	<100	<100	<100	<100	<100	<100	**<100**	100	4557306
Tungsten (W)	ppm	<1	<1	<1	<1	<1	<1	<1	**<1**	1	4557306
Uranium (U)	ppm	0.8	1.6	1.3	<0.5	<0.5	0.6	0.5	**1**	0.5	4557306
Ytterbium (Yb)	ppm	<0.2	<0.2	<0.2	<0.2	<0.2	0.2	0.3	**0**	0.2	4557306
Zinc (Zn)	ppm	<50	<50	<50	<50	<50	<50	<50	**<50**	50	4557306

Table 4. Raw results from Multi-Element Neutron Activation Analysis of seven samples from various depths of well FC77-1 provided by Maxxam Analytics, a subcontractor for Bureau Veritas Minerals.

Order 2 - FC79-18 (Reference Knox) - INAA										
	UNITS	79-18-71-A.1	79-18-73-A.1	79-18-74-A.1	79-18-75-A.1	79-18-76-A.1	79-18-77-A.1	**Average**	Reportable Detection Limit	Quality Control Batch
Bromine	ppm	1.1	1.1	1.8	0.8	0.7	0.7	**1**	0.5	4586476
Antimony (Sb)	ppm	<0.1	<0.1	<0.1	<0.1	<0.1	0.3	**0**	0.1	4586476
Arsenic (As)	ppm	2.1	1.5	1.1	1.1	2.5	5.1	**2**	0.5	4586476
Barium (Ba)	ppm	<50	<50	<50	<50	97	59	**78**	50	4586476
Calcium (Ca)	ppm	210000	190000	200000	210000	160000	190000	**193333**	10000	4586476
Cerium (Ce)	ppm	6	6	3	8	30	17	**12**	3	4586476
Cesium (Cs)	ppm	<1	<1	<1	<1	2	1	**2**	1	4586476
Chromium (Cr)	ppm	8	9	<5	6	21	12	**11**	5	4586476
Cobalt (Co)	ppm	<1	1	<1	<1	4	3	**3**	1	4586476
Europium (Eu)	ppm	<0.2	<0.2	<0.2	<0.2	0.4	0.2	**0**	0.2	4586476
Gold (Au)	ppm	<0.002	<0.002	<0.002	<0.002	<0.002	<0.002	**<0.002**	0.002	4586476
Hafnium (Hf)	ppm	<1	<1	<1	<1	<1	<1	**<1**	1	4586476
Iridium (Ir)	ppm	<0.005	<0.005	<0.005	<0.005	<0.005	<0.005	**<0.005**	0.005	4586476
Iron (Fe)	ppm	4200	4300	3900	4500	10000	8900	**5967**	100	4586476
Lanthanum (La)	ppm	2.4	2.8	1.1	3.3	13	7.3	**5**	0.5	4586476
Lutetium (Lu)	ppm	<0.05	<0.05	<0.05	<0.05	0.13	0.07	**0**	0.05	4586476
Mercury (Hg)	ppm	<1	<1	<1	<1	<1	<1	**<1**	1	4586476
Molybdenum (Mo)	ppm	<1	<1	<1	<1	<1	<1	**<1**	1	4586476
Neodymium (Nd)	ppm	<5	<5	<5	<5	13	9	**11**	5	4586476
Nickel (Ni)	ppm	<100	<100	<100	<100	<100	<100	**<100**	100	4586476
Rubidium (Rb)	ppm	<15	<15	<15	<15	43	27	**35**	15	4586476
Samarium (Sm)	ppm	0.5	0.4	0.3	0.6	2.2	1.3	**1**	0.1	4586476
Scandium (Sc)	ppm	1	1.2	0.2	1.2	4.5	2.9	**2**	0.1	4586476
Selenium (Se)	ppm	<3	<3	<3	<3	<3	<3	**<3**	3	4586476
Silver (Ag)	ppm	<5	<5	<5	<5	<5	<5	**<5**	5	4586476
Sodium (Na)	ppm	440	300	260	320	1000	650	**495**	100	4586476
Strontium (Sr)	ppm	<500	<500	<500	<500	<500	<500	**<500**	500	4586476
Tantalum (Ta)	ppm	<0.5	<0.5	<0.5	<0.5	<0.5	<0.5	**<0.5**	0.5	4586476
Terbium (Tb)	ppm	<0.5	<0.5	<0.5	<0.5	<0.5	<0.5	**<0.5**	0.5	4586476
Thorium (Th)	ppm	0.8	0.9	<0.2	0.8	3.2	1.7	**1**	0.2	4586476
Tin (Sn)	ppm	<100	<100	<100	<100	<100	<100	**<100**	100	4586476
Tungsten (W)	ppm	<1	<1	<1	<1	<1	<1	**<1**	1	4586476
Uranium (U)	ppm	0.6	0.6	<0.5	<0.5	1	1.2	**1**	0.5	4586476
Ytterbium (Yb)	ppm	<0.2	<0.2	<0.2	0.3	0.8	0.4	**1**	0.2	4586476
Zinc (Zn)	ppm	<50	<50	<50	<50	<50	<50	**<50**	50	4586476

Table 5. Raw results from Ultra Trace Geochemical aqua regia digestion analysis of six samples from various depths of well FC79-18 provided by Maxxam Analytics, a subcontractor for Bureau Veritas Minerals.